

D. W. Pierce · T. P. Barnett · N. Schneider
R. Saravanan · D. Dommenges · M. Latif

The role of ocean dynamics in producing decadal climate variability in the North Pacific

Received: 23 January 2000 / Accepted: 10 January 2001

Abstract Decadal time scale climate variability in the North Pacific has implications for climate both locally and over North America. A crucial question is the degree to which this variability arises from coupled ocean/atmosphere interactions over the North Pacific that involve ocean dynamics, as opposed to either purely thermodynamic effects of the oceanic mixed layer integrating in situ the stochastic atmospheric forcing, or the teleconnected response to tropical variability. The part of the variability that is coming from local coupled ocean/atmosphere interactions involving ocean dynamics is potentially predictable by an ocean/atmosphere general circulation model (O/A GCM), and such predictions could (depending on the achievable lead time) have distinct societal benefits. This question is examined using the results of fully coupled O/A GCMs, as well as targeted numerical experiments with stand-alone ocean and atmosphere models individually. It is found that coupled ocean/atmosphere interactions that involve ocean dynamics are important to determining the strength and frequency of a decadal-time scale peak in the spectra of several oceanic variables in the Kuroshio extension region off Japan. Local stochastic atmospheric heat flux forcing, integrated by the oceanic mixed layer into a red spectrum, provides a noise background from which the signal must be extracted. Although teleconnected ENSO responses influence the North Pacific in the 2–7 years/cycle frequency band, it is shown that some decadal-time scale processes in the North Pacific proceed without ENSO. Likewise, although the effects of stochastic atmospheric forcing on ocean dynamics are

discernible, a feedback path from the ocean to the atmosphere is suggested by the results.

1 Introduction

Significant decadal time scale climate variability has been observed in the North Pacific in a number of ocean and atmospheric variables (e.g., Miller et al. 1994; Trenberth and Hurrell 1994). Such variability has implications for both local ecology (Mantua et al. 1997) and wintertime temperatures and precipitation over North America (Latif and Barnett 1994). These are the time scales that encompass the effects of droughts and persistent crop failures, which can have severe economic and social impacts. Therefore, a successful prediction of such variability could potentially afford the opportunity to mitigate any otherwise damaging effects.

Such predictions of the future state of the climate system require at least two things; first, the nature of the mechanism or forcing giving rise to the variability must be understood if the applicability and limitations of the predictive strategy are to be quantified. Second, the mechanism itself must be a predictable process. It cannot be either intrinsically random, or chaotic in the sense that the initial conditions cannot be observed to a sufficient degree of precision to support the desired forecast lead time.

In this work we identify the mechanisms giving rise to North Pacific decadal time scale climate variability in a coupled ocean/atmosphere general circulation model (O/A GCM). Such variability can be thought of as arising three different kinds of ocean/atmosphere interaction: (1) stochastic heat flux forcing by the atmosphere that is integrated by the oceanic mixed layer, with only thermodynamics being important; (2) stochastic heat flux and wind stress forcing by the atmosphere that has a one-way effect on ocean dynamics, with no feedback to the atmosphere; (3) fully coupled, dynamical interactions between the ocean and atmosphere. The models do

D. W. Pierce (✉) · T. P. Barnett · N. Schneider
Climate Research Division, Scripps Institution of Oceanography,
La Jolla, CA, USA
E-mail: dpierce@ucsd.edu

R. Saravanan
National Center for Atmospheric Research,
Boulder, CO, USA

D. Dommenges · M. Latif
Max Planck Institute for Meteorology, Hamburg, Germany

not include other kinds of variable forcing that might be expected to have decadal time scales, such as solar variability, volcanism, or changes in anthropogenic greenhouse gases. These mechanisms are therefore not examined or discussed further here.

The effects of stochastic heat flux forcing on the midlatitude oceans was described by Hasselmann (1976) and Frankignoul and Hasselmann (1977), who noted that white-noise forcing of a damped oceanic mixed layer is integrated by the ocean to give a red spectrum for ocean temperatures (a review of this kind of work was presented in Frankignoul 1985). This was extended by Barsugli and Battisti (1998) to a more intrinsically coupled ocean/atmosphere system; they showed that coupling a stochastic atmospheric model to an oceanic mixed layer increases the low-frequency variance seen in both, as well as tending to reduce the heat exchanged between them. In the context of the present work, climate variability arising from this mechanism is of limited use for prediction, as it is intrinsically random in nature. The best that can be done is to quantify any implications of an observed anomalous state of the ocean mixed layer over the time that such an anomaly is expected to persist (for an example of this, see Gershunov and Barnett 1998).

Various dynamical ocean responses to stochastic atmospheric forcing have been examined by Frankignoul et al. (1997), Jin (1997), Saravanan and McWilliams (1998), Weng and Neelin (1998), and Munnich et al. (1998). Saravanan and McWilliams (1998) demonstrated that oceanic advection (for instance by a midlatitude gyre) underneath fluctuating atmospheric forcing that has a fixed spatial pattern can give rise to selective enhancement of the ocean variability at certain frequencies. Weng and Neelin (1998) pointed out that an atmospheric pattern of forcing with a preferred length scale (as is seen in the North Pacific) will give rise to a midlatitude oceanic Rossby wave response with the same preferred length scale, and hence to a preferred time scale via the Rossby wave dispersion relationship. Mathematically, these two mechanisms are similar; a water parcel's temperature or depth anomaly increases if it constantly experiences the same sign of forcing (either surface heat flux or wind stress curl) during its movement across a basin. In the Saravanan and McWilliams (1998) mechanism, the movement is accomplished by gyre transport, leading to an advective time scale; in the Weng and Neelin (1998) mechanism, the velocity and time scale are set by midlatitude Rossby wave dynamics. Frankignoul et al. (1997) gives a theoretical context for interpreting this work; with a monopole of forcing, no spectral peak is expected, but a peak (and hence preferred time scale) can develop if the atmosphere imposes a more complicated spatial pattern. These mechanisms do not need a feedback from the ocean to the atmosphere to select a time scale. However, if the atmosphere did respond to such oceanic changes (perhaps locally, or by a teleconnected effect that is not coincident with the ocean's original forcing

region), these mechanisms might produce potential predictability in the affected area if the state of the ocean could be well enough observed.

A fully coupled interaction between the ocean and atmosphere that requires ocean dynamics to operate was suggested by Latif and Barnett (1994, 1996). The hypothesized mechanism is that a spun-up Pacific subtropical gyre gives rise to warmer sea surface temperatures (SSTs) in the Kuroshio extension region, which may then feed back to the atmosphere in such a way as to spin down the gyre, decreasing the SSTs in the Kuroshio extension. Robertson (1996), using a different coupled GCM, identified an 18-year oscillation in the North Pacific that also appeared to be due to a coupled ocean/atmosphere processes, although that conclusion could not be made with absolute certainty.

In this work we analyze model results to identify which aspects of the midlatitude Pacific variability arise from each of these processes. The particular focus here is variability that arises from fully coupled ocean/atmosphere interactions and requires dynamical ocean processes, as these fluctuations are potentially predictable by numerical models. In the course of this analysis we will compare the results from fully coupled ocean/atmosphere models to results from full atmosphere models coupled to oceanic mixed layer models in order to determine the role of ocean dynamics. A similar analysis was done by Manabe and Stouffer (1996); in contrast to that work, which generally took a global and wideband view of the problem, we focus specifically on North Pacific interdecadal variability.

A preliminary overview of some of the results shown here was sketched out in Barnett et al. (1999b). Evidence was presented there showing that the North Pacific mode is stochastically driven by the atmosphere, while the preferential enhancement of variability at a time scale of 20 years/cycle seen in the Kuroshio extension region is due to internal ocean dynamics, and consistent with the mechanism suggested by Latif and Barnett (1994, 1996). The present work goes into more depth and detail than was possible there, and includes a fuller analysis of the forcing terms of the North Pacific mode, the relation of the North Pacific mode to cloudiness, a more complete investigation of the "time permuted" test runs used to examine the hypothesis that stochastic processes are the origin of the 20 year/cycle time scale, a different but complementary analysis of the OGCM runs examining the atmospheric response to imposed midlatitude SST anomalies, and a more thorough examination of the origin of the 20 year time scale.

This work is laid out as follows. In Sect. 2 we describe the models used in this study. The results are presented in Sect. 3, including the effect of ENSO on the North Pacific mode, influence of Ekman transport on the variability, the effect of ocean dynamics in the Kuroshio extension region, and a test of various mechanisms that have been hypothesized to give rise to interdecadal midlatitude variability. The results are discussed in Sect. 4, and conclusions are given in Sect. 5.

2 Model descriptions

A number of different numerical models are used in this work. The models used are summarized in Table 1 and described briefly. The specific intent of using these different models is *not* to perform a model intercomparison study, but rather to abstract out from the various model runs features that are common between them. An additional goal is to make use of ocean models of differing physical complexity coupled to a consistent set of atmospheric GCMs. Because of the various models used and differences in the variables saved in each model run, it is not always possible to achieve these goals. We emphasize the CCM3-based models when examining issues dealing with the mixed layer run, because there is data for exactly the same version of the atmospheric model coupled to both the mixed layer and full physics ocean models. Also, the depth of the mixed layer in the CCM3-based run is specified every month from observations, which will help give an accurate simulation; for the ECHAM-based models, ECHAM3 is used in the mixed-layer run but ECHAM4 in the full physics ocean run, and the depth of the mixed layer is fixed at 50 m; this is a less realistic setup than the CCM3-based mixed layer runs used. For the analysis of the full coupled ocean/atmosphere model, we analyze primarily the ECHO2 (ECHAM4 atmosphere/HOPE ocean) results, because we have a complete set of surface layer heat budget terms for this run; these terms are not available for the CSM (CCM3 atmosphere/NCOM ocean) run.

All models are global domain and have realistic topography. A complete description of the models' physics and base climatology can be found in the referenced works.

2.1 ECHAM atmospheric models

We use two European Center/Hamburg (ECHAM) atmospheric models, ECHAM3 (DKRZ 1992; Roeckner et al. 1992) and ECHAM4 (Roeckner et al. 1996). Both models are spectral and use a hybrid vertical coordinate scheme, with sigma levels near the surface that flatten to surfaces of constant pressure in the stratosphere. The highest level in both models is at a pressure of 10 mb; there are 19 layers. A time step of 24 min is used. The earlier version, ECHAM3, is used at a resolution of T21 in a configuration coupled to a mixed layer ocean model with a fixed depth of 50 m.

ECHAM4 added a semi-Lagrangian scheme for transporting water vapor, cloud water, and trace substances, and a closure for deep convection based on convective instability rather than the moisture convergence criterion used in ECHAM3. It is used here at T42 resolution, both stand alone and coupled to a full oceanic model, HOPE version 2.4 (described later). The coupled run with ECHAM4/HOPEv2.4 is known as ECHO2, and described in Frey et al. (1997), Pierce et al. (2000), and Venzke et al. (2000a). (Note that Latif and Barnett 1994, 1996 used ECHO1, which is ECHAM3 coupled to HOPEv1). Because we have the most complete set of data for ECHO2, including surface heat budget terms, it will be the focus of our work.

2.2 CCM3 atmospheric model

The Community Climate Model, version 3 (CCM3; Kiehl et al. 1996) is used here in a long run coupled to the full physics NCAR Ocean Model (NCOM) in the experiment known as "b003", as well

as joined to a slab ocean model. In coupled form, CCM3/NCOM is termed the Climate System Model (CSM), and described by Boville and Gent (1998; see also the CSM special issue of *J. Climate*, vol 11, 6). CCM3 is a spectral model that uses a terrain-following vertical coordinate system with 19 vertical levels, and is used here at a resolution of T42. A shape-preserving semi-Lagrangian scheme is used for horizontal transport of water vapor, cloud water variables, and chemical constituents. The slab ocean model incorporates mixed layer ocean physics, with the mixed layer depth set from observations (Levitus 1994).

2.3 NCOM ocean model

The NCAR ocean model (NCOM; NCAR 1997) is a primitive equation level ocean model that is derived from the Modular Ocean Model, version 1.1 (Pacanowski et al. 1993). It uses 45 vertical levels, with four levels in the top 50 m. The horizontal resolution is 2.4° in longitude and variable resolution in latitude, with a minimum spacing of 1.2° at the equator and a maximum of 2.3° in midlatitudes. The Gent and McWilliams (1990) eddy mixing parametrization is used, as well as a nonlocal K profile boundary layer parametrization (Large et al. 1994) to improve the simulation of the oceanic mixed layer. A third order upstream differencing scheme is used for temperature and salinity (Holland et al. 1998).

2.4 HOPE ocean model

The Hamburg Ocean Primitive Equation (HOPE) model is a primitive equation ocean model formulated on levels (Wolff et al. 1997). It is implemented on an Arakawa E-grid (Arakawa and Lamb 1977) with finer latitudinal resolution in the tropics, 0.5° between 10°S and 10°N, to give better fidelity to the simulation of ENSO processes. The overall number of horizontal gridpoints is 130 by 121, with 20 vertical levels (top level thickness is 20 m). Horizontal mixing has both Laplacian and biharmonic components. Vertical mixing is based on a Richardson-number dependent scheme. At the top of the water column, layers within 0.5 K of the surface temperature are subjected to increased vertical mixing to represent the effects of stirring by the wind (Latif et al. 1994).

3 Results

3.1 The North Pacific mode and ENSO

As has been pointed out by many researchers (e.g., Horel and Wallace 1981; Blackmon et al. 1983; Graham et al. 1994) the ENSO cycle has a teleconnected expression in the North Pacific. For our purposes, the relevant question is to what degree decadal time scale variability in the North Pacific is associated with ENSO, as opposed to being a local midlatitude phenomenon. This has important implications for how a prediction scheme for the North Pacific should work; if the response arises exclusively from a teleconnected ENSO response, a prediction scheme for the North Pacific

Table 1 Coupled models used in this study. All are global domain

Model	Atmosphere	Ocean	Resolution	Number of years
ECHO2	ECHAM4	HOPE 2.4	T42	137
CSM	CCM3	NCOM	T42	270
ECHAM3/ML	ECHAM3	Mixed layer, 50 m	T21	170
CCM3/ML	CCM3	Mixed layer, depth from Levitus	T42	100

should be essentially a prediction scheme for ENSO (perhaps coupled to a extratropical oceanic mixed layer model). If part of the low-frequency North Pacific variability proceeds independently of ENSO, then the local midlatitude dynamics that generate this variability must be correctly modeled as well.

This question has previously been addressed in a linear framework by statistical analysis of observations. Deser and Blackmon (1995) found that the two leading empirical orthogonal functions (EOFs) of SSTAs in the wintertime Pacific correspond to an ENSO mode (which explains 43% of the variance), and a North Pacific mode with little expression in the tropics, generally being confined between 20°N and 60°N (11% of the variance). They noted that the two modes are linearly independent, and tend to have a different temporal character. Zhang et al. (1996) performed a similar analysis, using an ENSO index to remove (by linear regression) the tele-connected ENSO signal from the North Pacific, and demonstrating that the residual corresponds to Deser and Blackmon's (1995) North Pacific mode. Thus both these studies support the idea that there is an mode of variability in the North Pacific that is independent of the teleconnected ENSO response.

One contribution of the present work is to address this question in a non-linear dynamical framework, by using specific numerical experiments that lack ENSO. To remove ENSO, defined here as a coupled ocean/atmosphere phenomenon that requires both ocean and atmosphere dynamics, we make use of model runs ECHAM3/ML and CCM3/ML, which have full-physics atmospheric models coupled to simplified, mixed-layer ocean models that lack dynamics. The result is model runs that still have tropical ocean SST variability (naturally enough, since SSTs are not fixed in the region), but whose tropical SST variability does not arise from ENSO processes per se. The question of what remains in the North Pacific without ENSO can thus be addressed using the full, non-linear dynamics of an atmospheric GCM.

Figure 1 shows the results, given in terms of EOFs of SSTA taken over the winter months (November to March). For comparison, the top panel shows the second EOF of observed SSTAs, taken from da Silva et al. (1995) over the period 1945 to 1982 and blended with NCEP SSTs over the period 1983 to 1999. The result is similar to that obtained by Deser and Blackmon (1995): a central lobe of one sign extending out along 40°N, surrounded by loadings of the opposite sign in a horseshoe shaped pattern along the west coast of North America. The middle panel shows the leading EOF from the ECHAM3/ML run; the bottom panel shows the leading EOF from the CCM3/ML run. The percent of explained variance in the models is 16% and 25.5% for ECHAM3/ML and CCM3/ML, respectively, compared to the 11% Deser and Blackmon (1995) found for the observed mode.

The models that have only ocean thermodynamics, and no ocean dynamics, evolve leading EOFs (lower two

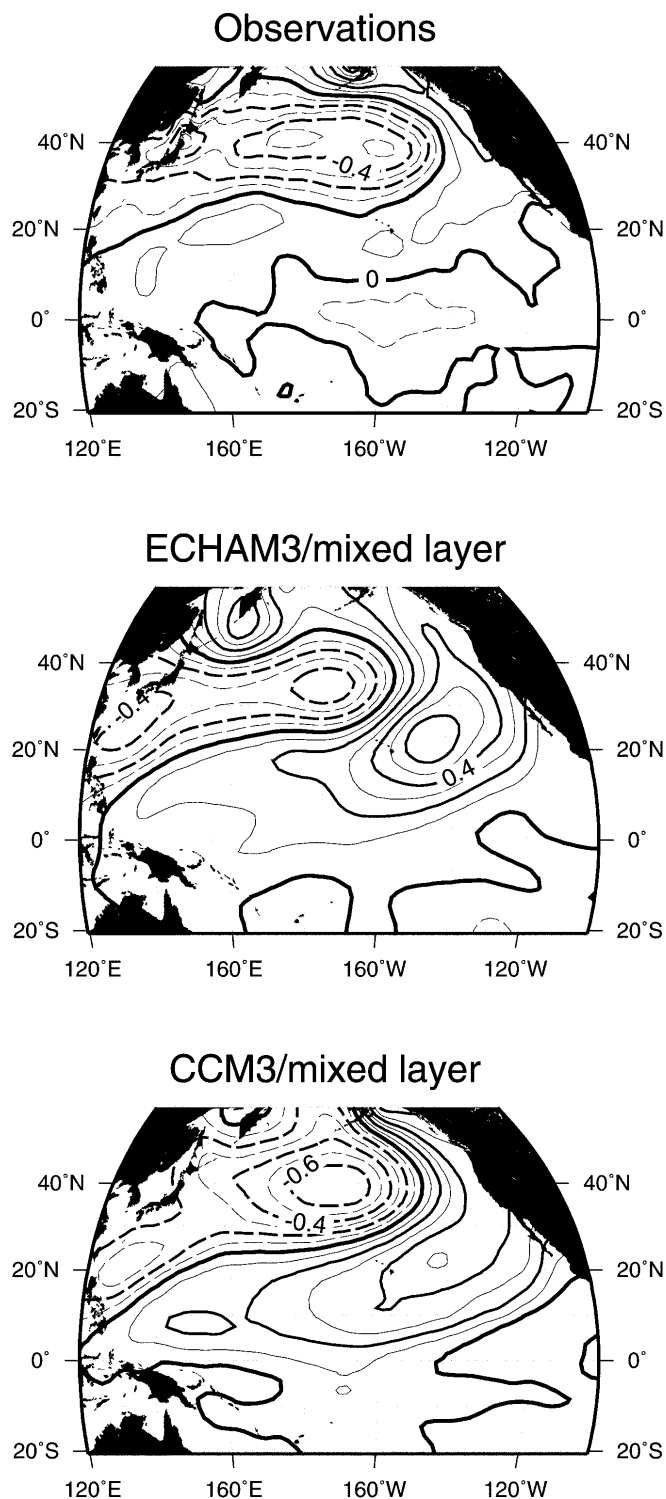


Fig. 1 EOFs of SSTA over the cold season (November to March). *Top*: second EOF from observations, 1945 to 1999. *Middle*: leading EOF from ECHAM3 AGCM coupled to a mixed layer ocean model. *Bottom*: leading EOF from CCM3 AGCM coupled to a mixed layer ocean model. Contour level is 0.1 K per standard deviation of the associated principal component

panels) that are similar to the observed pattern (top panel). The central lobe extending out from Japan is well defined in the model runs (although a few degrees too far

south in ECHAM3/ML), and the surrounding horse-shoe shaped region of opposite loading is present in both the mixed layer runs. For unknown reasons both mixed layer runs have more loading in the region around 22°N, 142°W than is observed. Nonetheless, the similarity of the mixed layer ocean models to the observations demonstrates that the major features seen in the observed EOF are obtainable without either teleconnected ENSO forcing or ocean dynamics.

The latter point deserves further comment. This pattern is found in the observations and in atmospheric models coupled to fully dynamic ocean models. However, since this characteristic pattern of SSTAs is obtained even in the absence of ocean dynamics, in the mixed layer runs it must arise exclusively from the ocean's thermodynamic response to atmospheric forcing. It might be conjectured that the geographical distribution of the pattern is set by atmospheric forcing, but that dynamical feedbacks between the ocean and atmosphere could amplify the strength of the pattern (such as happens with ENSO, see Barnett et al. 1993). However, the contour values shown in Fig. 1 are normalized to show the amplitude of the pattern, in K, for a one standard deviation excursion of the associated principal component (PC). It can be seen that the amplitude of the pattern in the mixed layer runs is remarkably similar to that observed, about 0.4 to 0.5 K. This is not consistent with the idea that a dynamical feedback is required to amplify the strength of the pattern; rather, both the strength and geographical distribution of the pattern are reasonably well captured even in the absence of ocean dynamics.

The spectra of the PCs associated with the EOFs of Fig. 1 are shown in Fig. 2, along with the 95% confidence intervals based on a best-fit AR(1) spectrum. (Note that the confidence intervals are different for the different data sets, as they depend on the number of years analyzed: 52, 169, and 99, respectively, from top to bottom). Although all spectra show power at the interdecadal time scales, none show significantly more than would be expected were the processes strictly AR(1) with noise forcing, as would be expected for this purely thermodynamic case from the arguments of Hasselmann (1976). The CCM3/ML spectrum (bottom panel) approaches the 95% confidence limit at a frequency of ≈ 0.24 cycles/year, but examination of the spectra of SSTAs in the tropical region verified that no similar spectral density enhancement is found in tropical SSTAs at this frequency; hence, all indications are that this is a chance fluctuation.

The conclusion to be drawn from this is that the pattern shown in the top panel of Fig. 1, and identified by Deser and Blackmon (1995) as the “North Pacific mode”, can indeed be created independently of ENSO effects. Furthermore, it can appear even in the absence of ocean dynamics. In the observations as well as the atmosphere/ocean mixed layer models, the North Pacific mode has a red spectrum with no significant peaks. This evidence therefore supports the idea that the North

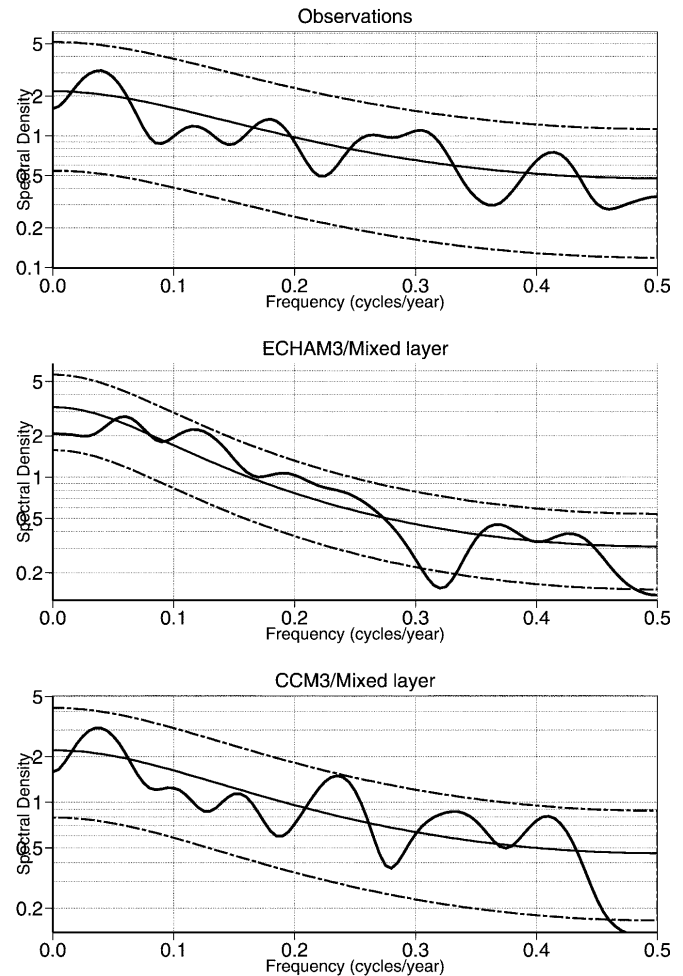


Fig. 2 Spectra of the principal components for the EOFs shown in Fig. 1, from observations, ECHAM3/mixed layer ocean, and CCM3/mixed layer ocean (*top to bottom*). Also shown are the best fit AR(1) spectra and associated 95% confidence limits (*dashed*)

Pacific mode is stochastically driven by the atmosphere, with heat fluxes thermodynamically integrated by the ocean's mixed layer.

The definition of ENSO used here, one that requires ocean dynamics and therefore can be properly removed using a non-dynamical ocean model, leaves intact other aspects of tropical variability that might be conjectured to play a part in forcing the North Pacific mode. The role of this non-ENSO tropical variability is addressed in Sect. 4.

3.2 The North Pacific mode and Ekman transport

As described in Sect. 3.1, evidence from the CCM3/ML and ECHAM3/ML runs support the idea that the main geographical characteristics of the North Pacific mode are set by stochastic atmospheric forcing of the ocean's mixed layer, and do not require dynamical ocean processes. Nonetheless, Ekman currents driven by the atmospheric variability associated with the North Pacific

mode would be expected to modify this pattern. This issue will now be addressed by comparing the surface heat budget in the ECHAM3/ML run, which lacks ocean dynamics, to the ECHO2 run, which includes such dynamics. The analogous analysis cannot be made for the CSM run because of the lack of surface heat budget terms from that run.

The analysis will be done here in terms of a canonical correlation analysis (CCA), using the components of the ocean's surface heat budget as the predictor and December-to-December temperature tendency as the predictand. CCA is a linear regression technique used here to find the most strongly correlated coexisting patterns of temperature tendency and surface heat budget terms (see Barnett and Preisendorfer 1988, for further details on the technique). Figure 3 shows the results of the CCA analysis on the ECHAM3/ML run. Note that this model has no transport terms or anomalous vertical mixing in the surface heat budget. The predictors are the top four panels of the figure; the predictand, temperature tendency, is the bottom panel. The similarity between the leading mode of temperature tendency (bottom panel) and the North Pacific mode of SSTA (Fig. 1, middle panel) confirms that the CCA is picking out the North Pacific mode for the analysis. The latent heat flux is the dominant surface heat balance component determining

the geographical signature of the North Pacific mode, contributing about $30\text{--}40\text{ W/m}^2$ for one standard deviation of the predictor time series, with its tongue of one sign extending out from Japan surrounded by loading of the opposite sign. The influence of the solar component can also be seen to contribute about $10\text{--}20\text{ W/m}^2$, while the sensible and longwave components have little effect. The overall result is in accordance with the results of Sect 3.1, the distinctive pattern of the North Pacific is set by stochastic atmospheric forcing primarily effected via the latent heat flux, with some contribution from changes in insolation. By regressing for the observed wind speed field associated with the North Pacific mode, Deser and Blackmon (1995) suggested that the latent heat flux might be the dominant driving term. Here, having the budget terms available from a numerical run allows us to confirm the role of the latent heat flux, as well as pointing out the modifications due to the solar heat flux component.

When ocean dynamics are added to the picture, the effects of Ekman transport can be discerned. This is shown in Fig. 4, which presents a similar CCA analysis using the ECHO2 run. Again, the upper panels show the various components of the surface heat balance as predictors; the lower panel shows the temperature tendency as a predictand. The latent, sensible, solar, and longwave

Fig. 3 The leading mode from a CCA analysis of the ECHAM3 AGCM coupled to a mixed layer ocean model. The *top four panels* are the predictors, components of the surface heat budget, with a contour level of 5 W/m^2 ; the *bottom panel* is the predictand, temperature tendency, with a contour level of 0.1 K

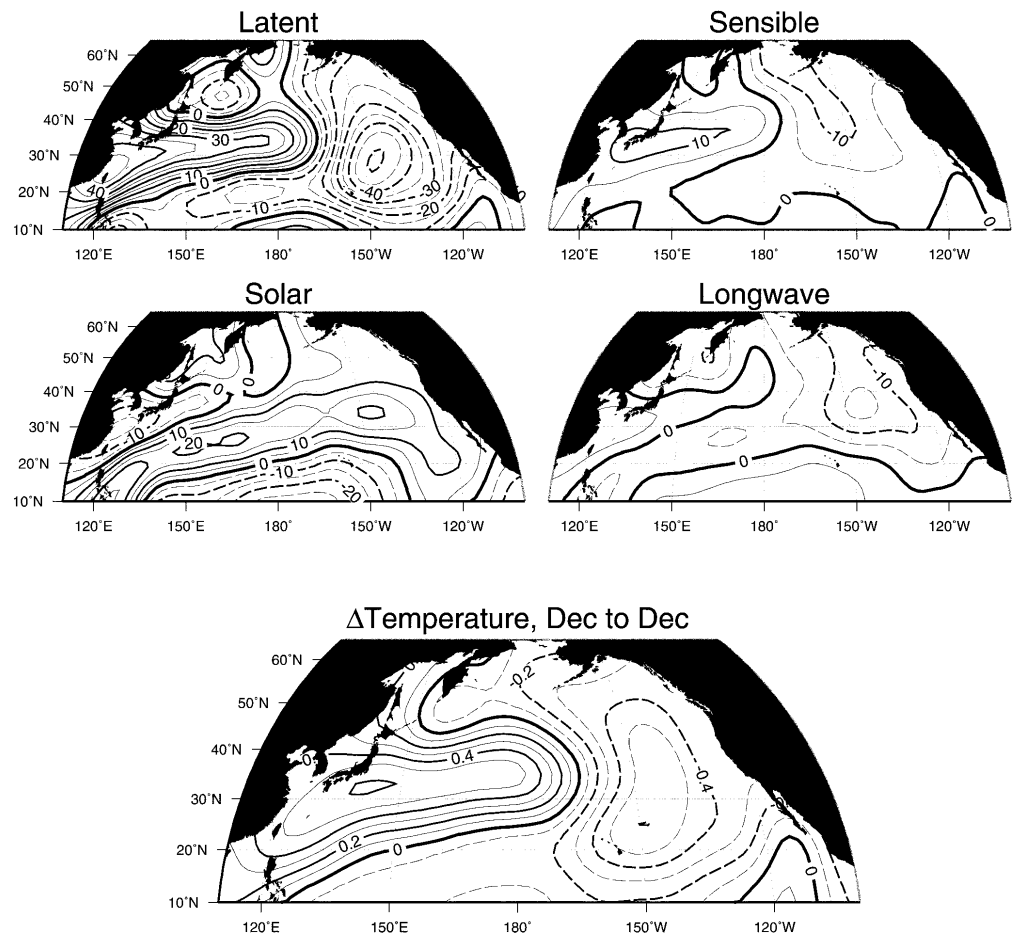
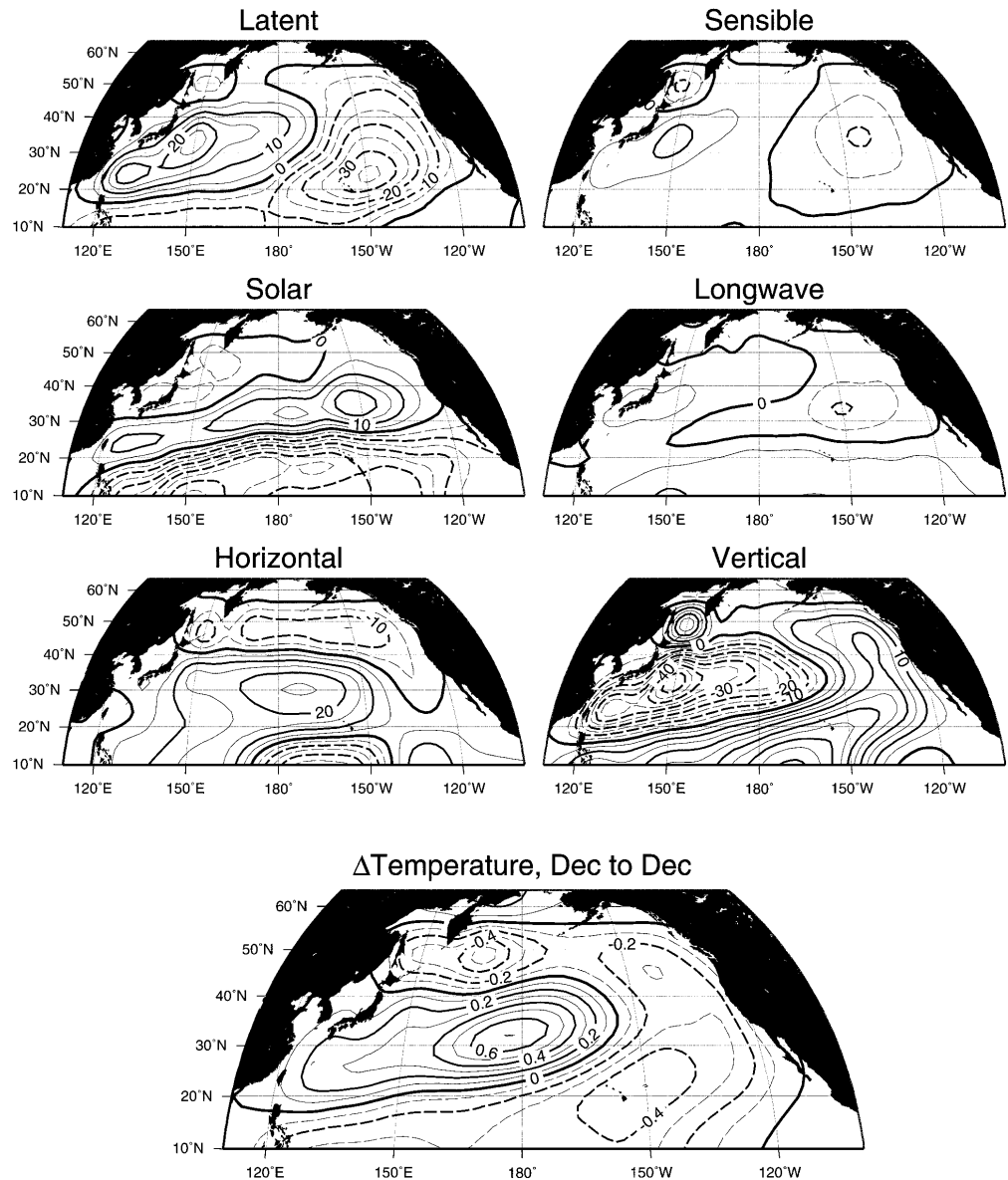


Fig. 4 As in Fig. 3 but for the ECHAM4 AGCM coupled to the full physics HOPE ocean model. The *top six panels* are the predictors; the *bottom panel* is the predictand



components show only minor differences from the case with no ocean dynamics. The new surface terms, applicable to the surface gridbox only (20 m thick), are the horizontal, which incorporates both horizontal advection and mixing; and the vertical, which includes vertical advection and convective mixing. The primary heat balance in the surface gridbox is atmospheric forcing by the latent heat flux balanced by vertical convective mixing out of the surface gridbox (note that the sign of the latent heat flux matches the sign of the temperature tendency, while the vertical component is of the opposite sign). In a sense this is a less interesting balance than it could be, because the heat budget components are only available in the top model gridbox, rather than integrated over the mixed layer. The main function of the vertical component here is to distribute the atmospheric signal into the rest of the oceanic mixed layer (see Miller et al. 1994, for a more thorough investigation of the role

of vertical mixing in low-frequency North Pacific variability).

The horizontal component is dominated by the heat flux associated with the Ekman transport. The atmospheric state associated with the North Pacific mode is that of an anomalous high pressure over warm temperatures in the central North Pacific (as has been pointed out by, e.g., Latif and Barnett 1994). This is associated with anomalous anti-cyclonic circulation, which tends to move cold, subpolar water southwards in the northern part of the Pacific, and move warm, subtropical water northwards in the southern part of the Pacific. The result is the bipolar pattern seen in the horizontal component of Fig. 4, with net cooling north of net warming. A linear regression between the predictor time series of Fig. 4 and the wind stress field (not shown) indicates that the surface wind stress anomalies associated with this Ekman transport are about 0.007–0.01 Pa for one

standard deviation of the predictor time series. This is $O(10\%)$ of yearly averaged climatological wind stress values in the region.

3.3 The North Pacific mode and cloudiness

The results from the model runs ECHAM3/ML (Fig. 3) and ECHO2 (Fig. 4) indicate that the North Pacific mode is associated with changes in solar forcing as well as in latent heat flux. Can this model result be verified from the observations? In an attempt to address this, Fig. 5 shows the correlation map between observed yearly averaged SSTA, over the period 1965–1993, in a box centered on 160°W, 39.5°N (in the region of high loading for the SSTA EOF; see the top panel of Fig. 1) and observed yearly averaged solar heat flux anomaly during the same period from observations (da Silva et al. 1995). The idea here is to use the SSTA index as proxy for a North Pacific mode index, so the correlation map will show what solar heat flux is associated with the North Pacific mode. An autocorrelation of solar heat flux in the central Pacific shows no relationship at lags greater than one year, suggesting that the proper number of degrees of freedom for this correlation is 29, by which values are significant at the 95% level if their magnitude exceeds 0.32. Regions where this is true are shaded in the figure. The central features produced by the models, a band of anomalous negative forcing south of about 25°N, then a band of positive forcing north to about 40°N, with both bands sloping poleward towards the east, are present in the observations as well, lending credence to the model results. Note that this association does not imply that SST anomalies are forcing cloud cover anomalies; it is reasonable to suppose that the stochastic atmospheric variability has expression in cloudiness and also forces changes in the surface latent heat flux, both of which then affect SSTs.

The changes in ECHO2 cloudiness associated with this change in solar forcing can be found by compositing total cloudiness upon extremes of the predictor time series from Fig. 4. As expected, the results (not shown) have a pattern similar to that in the “Solar” panel of Fig. 4, but with opposite sign (more clouds over regions

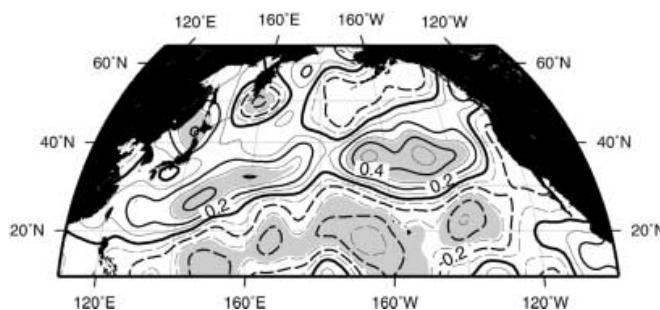


Fig. 5 Correlation map, from observed data, between SSTA centered on 160°W, 39.5°N and yearly-averaged solar flux anomaly at every point. *Shaded regions* are significant at the 95% level

with less surface solar heating). Taking the difference between the top and bottom 20th percentiles of the predictor time series shows differences in yearly averaged fractional cloudiness of 3–5% over the affected region (170°E to 120°W, 15°N to 35°N).

3.4 Effects of ocean dynamics in the Kuroshio extension

The previous results show the importance of stochastic atmospheric forcing and Ekman transport to the North Pacific mode. Where, then, do oceanic dynamics exclusive of Ekman transports play a role? A straightforward way of determining this is to divide, at each point, the variability in a model run with an AGCM coupled to a full physics ocean model to the same AGCM coupled to a mixed layer ocean model. The results of doing this are shown in Fig. 6, where the variability is illustrated by means of the ratio of spectral density of SSTAs. The models used are CSM and CCM3/ML; these particular two runs were chosen to form the ratio because they have the same atmospheric model at the same resolution, and the mixed layer ocean depth (in the mixed layer run) is specified from observations. Forming this ratio from runs that use different atmospheric models (i.e., the ECHAM3/ML and ECHO2 runs) is not as uniform a comparison, although this is attempted in Fig. 9 for completeness. The ratio is shown at various frequencies from 20 to 5 years per cycle. The statistical significance of the result can be assessed by noting where the 90% confidence intervals of the two spectra used to form the ratio do not overlap; such regions are shaded on the figure.

There are two bands where ocean dynamics significantly increases SST variability in the model: an interdecadal band of about 20 years/cycle and the ENSO band centered at about 3.6 years/cycle (not shown). Furthermore, each frequency band is associated with a specific spatial distribution of enhanced variability. The increase in variability associated with the ENSO band is concentrated in the tropics, as is well known. The increase in the interdecadal band is primarily in the extratropical North Pacific, with centers in the sub arctic frontal zone (SAFZ)/Kuroshio extension region off Japan as well as off the Aleutian islands. The CSM model develops anomalous and unrealistic sea ice in the Aleutian island center of variability; we assume that the variability in this region is associated with this model error (or, at least, not practicably separable from it), and so is not examined further.

Figure 7 shows the ratio for all frequencies, at the point 155°W, 43°N (in the model’s SAFZ). Shaded regions show where the 90% confidence intervals for the two spectra used to make the ratio do not overlap. The ratio is strongly peaked at a frequency of about 20 cycles/year, with a minor subsidiary peak at about 6 cycles/year but little else besides. The implication is clear: ocean dynamics preferentially enhances variability

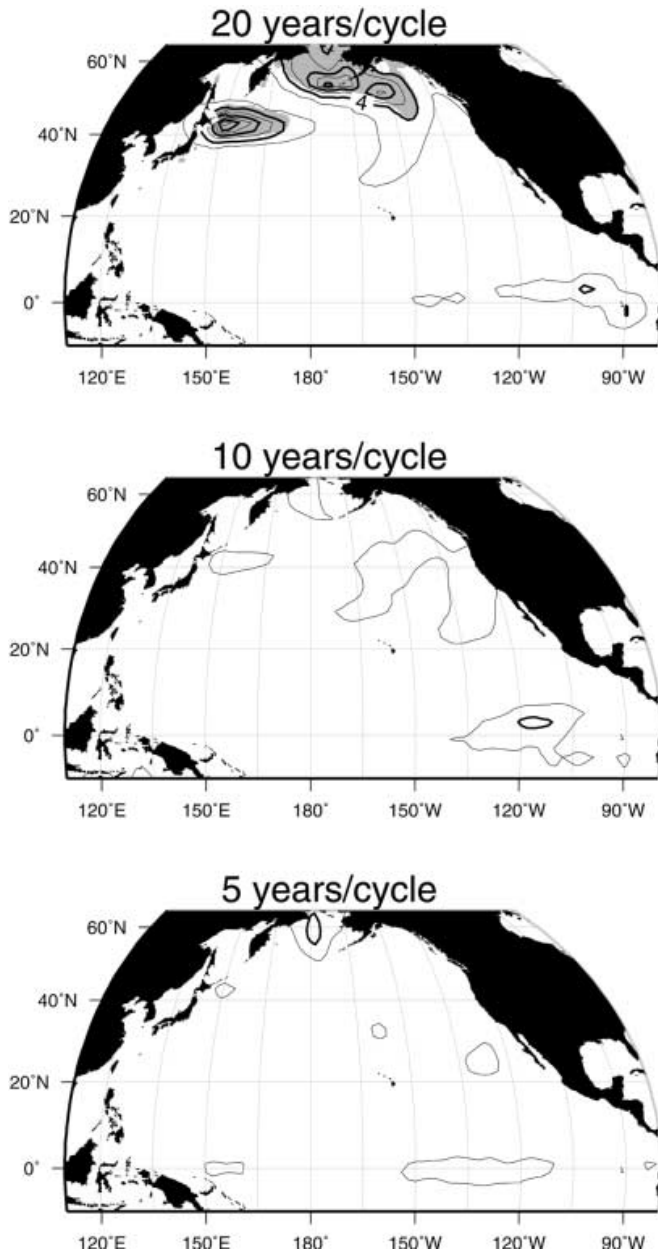


Fig. 6 Ratio of spectral density, at various frequencies, in the CSM full physics O/A GCM run to a run with the CCM3 AGCM coupled to a mixed layer ocean model. Contour interval is 2. Shaded areas show where the ratio is statistically significant (see text for details)

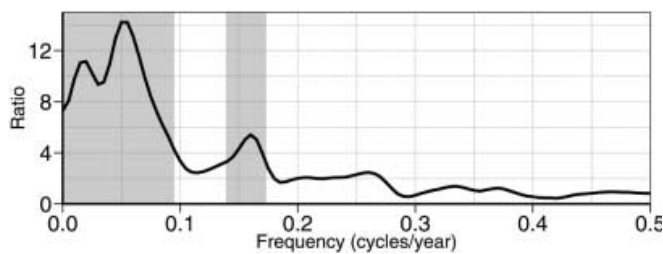


Fig. 7 Ratio of spectral density in CSM to that in CCM3/ML, at the point 155°W, 43°N. Shaded areas show where the ratio is statistically significant (see text for details)

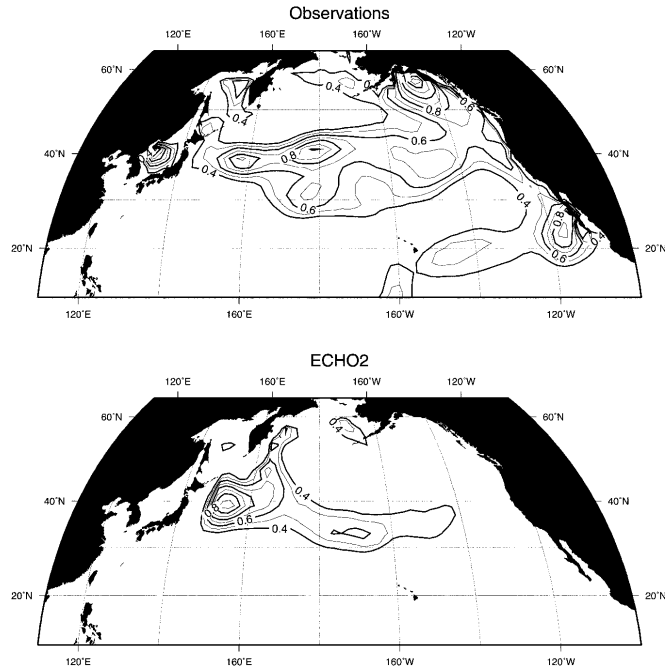


Fig. 8 Spectral density of SSTA at a frequency of 20 years/cycle for observations over the period 1945–1993 (top) and the ECHO2 model (bottom)

in the SAFZ/Kuroshio extension region and at the interdecadal frequencies, rather than forcing a broadband response. An intimation of this can be seen in Manabe and Stouffer (1996), their Fig. 9, which shows SST standard deviation in this region is enhanced by about a factor of 2 in the presence of ocean dynamics. However, it is really only when the variability as a function of frequency is examined (Fig. 7) that the full extent of this enhancement becomes clear.

Since the real oceans incorporate the effects of ocean dynamics, an exact analogue to Fig. 6 cannot be made from observed data. However, a less direct (but still useful) comparison can be done by simply plotting the geographical distribution of SSTA spectral density at the frequency of interest, 20 years/cycle here. This is shown in Fig. 8 for the observed data from 1945 to 1993 (da Silva et al. 1995), along with the same quantity from the ECHO2 model for comparison. The same plot for CSM looks similar to the upper left panel of Fig. 6, and so is not repeated here. In the observations, there is a region in the central Pacific of enhanced interdecadal variability, as seen in the models, but both models consistently trap the variability more towards the coast of Japan than is observed. The observations also show a strong signal off the west coast of North America that the models lack. An important caveat to keep in mind is that the 49 years of observed data can yield at most 2.5 cycles at a frequency of 20 years/cycle; the sampling issues associated with the observed data can hardly be overstated. Nonetheless, proceeding with what we have, we tentatively conclude that the observed data is roughly consistent with the model indications that preferential

enhancement of low-frequency variability occurs in the SAFZ/Kuroshio extension region. This effect is seen farther west in the models than in the observations, which suggests consistent model errors in the ability to advect signals along the axis of the Kuroshio current (which is represented only approximately in these medium resolution models). The reason for the discrepancy off the west coast of North America, and the implication this has for model errors, is not currently known. One possibility is that it is related to small-scale eastern boundary dynamics, such as coastal upwelling, which is known to occur in the region but cannot be properly resolved with the models used here.

The variability ratio shown in Fig. 7 made use of CSM and CCM3/ML, as they are the two most similar runs for the purposes of this comparison. However, we would like to look at the interdecadal response in ECHO2, as this is the run for which we have the most complete surface heat budget diagnostics. To that end, Fig. 9 shows a similar plot of spectral density ratios of SSTA in the Kuroshio extension, but using ECHO2 divided by ECHAM3/ML. Shading, indicating statistical significance, is as in Fig. 7. Note that in this case the ratio is taken at a latitude of 40°N ; the ECHAM models have the peak response one gridpoint south of the CCM3 models. The geographical distribution of enhanced variability is similar to that seen in CSM, with the exception that no regional maximum is seen in the Aleutian Island region. This is consistent with the idea that CSM's maximum in the region is related to the anomalous ice there.

The tail of the ratio at high frequencies tends to a value of about one-third, rather than about one, as found in Fig. 7. Manabe and Stouffer (1996) (their Fig. 4) find that ocean dynamics over the bulk of the North Pacific decreases variability by 10–20%, in rough agreement with Fig. 7 but nowhere near enough to explain the factor of three found in Fig. 9. From this we can conclude that either ECHAM3 has about three times as much intrinsic low frequency variability as ECHAM4, or that the fixed mixed layer depth of 50 m used in the ECHAM3/ML run is acting to exaggerate the low frequency variability by a factor of three. The latter conjecture is supported by the observation that the mixed layer depth in ECHO2 is about 150 m in

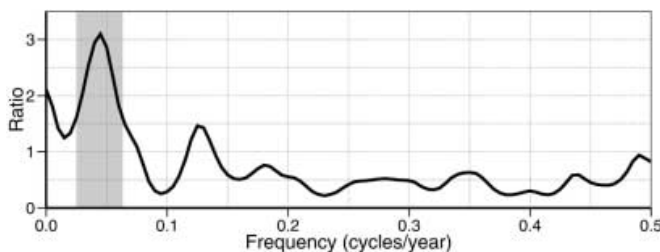


Fig. 9 Ratio of spectral density in ECHO2 to that in ECHAM3/ML, at the point 156°W , 40.5°N . Shaded area shows where the ratio is statistically significant (see text for details)

the SAFZ, and hence (all other things being equal) we expect to see the ECHAM3/ML run overstating the SST variability by a factor of three. Since this is what we observe in the models' behavior, we take this as the proper explanation for the discrepancy. Scaling the peak in Fig. 9 by a factor of three because of the mixed layer depth difference, we estimate that in ECHO2, ocean dynamics enhances low frequency variability in the Kuroshio extension region by a factor of 9. This enhancement happens preferentially at a frequency of about 22 years/cycle. This is roughly consistent in frequency with the results of the CCM3 model, although less than the enhancement seen in CCM3. Thus, based on both the ECHAM and CCM3 series of models, we conclude that ocean dynamics acts to increase interdecadal (~ 20 years/cycle) variability of SST in the Kuroshio extension region off Japan by about an order of magnitude.

A further dynamical consistency check of this conclusion can be made. If the enhancement in SST variability off Japan is due to dynamical processes, one would expect various oceanic quantities that are inter-related through the dynamics (for example, stream function and heat content) to all show the same spectral enhancement at the same frequency. This can be checked in the case of ECHO2; Fig. 10 shows the spectral density of five oceanic quantities in the SAFZ region of ECHO2. The intent of using five different quantities is to avoid identifying as significant peaks that exceed 95% significance merely by chance, due to sampling fluctuations. The spectra have all been pre-whitened by a best fit AR(1) process, then normalized so that they can be directly compared. All the quantities show a spectral peak that exceed the 95% confidence level at a frequency ~ 20 years/cycle. There are various other frequencies at which one or the other of the spectra exceeds the 95%

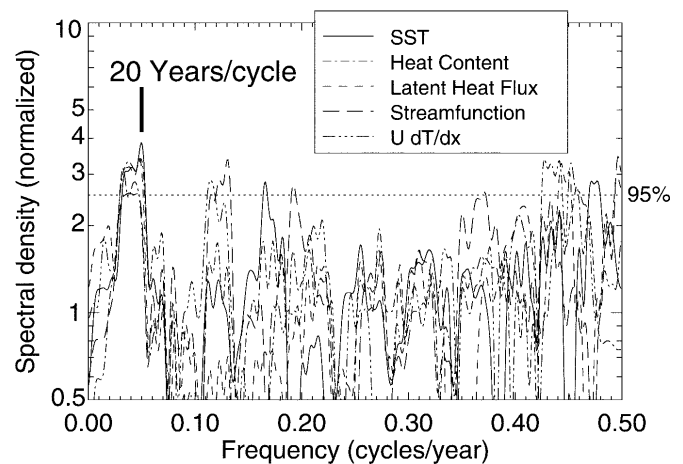


Fig. 10 Normalized and pre-whitened power spectra of various ocean quantities in ECHO2 in the Kuroshio extension region. *Solid line*: SST. *Dash-dot*: heat content, integrated to 1000 m. *Short dashes*: surface latent heat flux. *Long dashes*: barotropic streamfunction. *Dash-dot-dot-dot*: advection of zonal temperature gradient by the zonal velocity

threshold, but such would be expected to happen 5% of the time just by chance. The fact that only at ~ 20 years/cycle do all the spectra have a common peak lends strong support to the idea that this peak is not a statistical fluke, but rather is a real, dynamically consistent feature of the system. It is likely that the effects of dynamics are most easily seen in this region because of the strong meridional temperature gradients coupled with the nature of western boundary regions to reflect the integrated effects of all forcing to the east.

The importance of removing the best-fit AR(1) spectrum before computing Fig. 10 deserves to be emphasized. The majority (56% in ECHO2) of the interdecadal spectral power enhancement in the Kuroshio extension region due to ocean dynamics can be accounted for by the removed AR(1) process (see Frankignoul et al. 1997). This part is not our primary interest here, as we are more concerned with detecting the spectral signatures of a coupled mode that rise above an AR(1) background. Nonetheless, it should be kept in mind that this is the smaller portion of the entire enhancement of variability that arises from ocean dynamics.

3.5 Physical mechanisms for an interdecadal spectral peak

For the purpose of making predictions, it is important to know the cause of the interdecadal peak seen in ECHO2. Several previous workers have described mechanisms that might produce a low-frequency spectral peak in a midlatitude ocean of the kind seen here. These mechanisms will now be described, and then tested to see if they are the cause of the spectral peak in the Kuroshio extension region found in the ECHO2 model.

3.5.1 Advective resonance

Saravanan and McWilliams (1998) suggested that preferential enhancement of variability at a certain frequency could occur if oceanic advection proceeds underneath a region with a characteristic spatial pattern of atmospheric forcing, a process that will be referred to here as “advective resonance”. Such conditions are found in the North Pacific, where the subtropical and subpolar gyres circulate beneath the surface pattern of forcing associated with the stochastically driven North Pacific mode (see Sect. 3.1). The advective resonance mechanism has SSTAs being amplified by virtue of experiencing the same sign of atmospheric forcing as they are advected around the gyre. As a result, there should be a tendency for a positive correlation between net surface heat flux and SSTAs (using the sign convention that positive heat flux anomalies increase SST). A direct test of this found that the correlation between these two quantities over the North Pacific subtropical gyre was weakly negative, and not statistically signifi-

cant. This is not consistent with the advective resonance mechanism.

It might be hypothesized that the relationship between SSTA and net surface heat flux suggested by the advective resonance mechanism would have a regional character, with most of the forcing happening in the central gyre and most of the opposite-signed damping occurring in the western boundary region. Separating the gyre domain into two regions, the central gyre and the western boundary/Kuroshio extension region, and performing the same correlation analysis shows this to be partially true; most of the atmospheric damping of SSTAs occurs in the Kuroshio extension region, as determined by the strong negative correlations between SSTA and net surface heat flux in that region (not shown). However, using only data from the central gyre to perform the correlation again shows no statistically significant values. We therefore conclude that advective resonance is not causing the interdecadal-frequency spectral peak seen in the ocean variables of ECHO2 off Japan. A further test of this possibility, using a different technique than simple correlation analysis, is performed in the next section.

3.5.2 Stochastic excitation of Rossby waves

Weng and Neelin (1998) suggested that a preferred spatial scale for atmospheric forcing would result in the same preferred spatial scale being imposed on the oceanic Rossby wave response, and therefore, lead to a preferred oceanic time scale via the Rossby wave dispersion relationship. For the cases they studied (similar to the midlatitude North Pacific) the expected time scale for spectral enhancement should be in the interdecadal frequency band. A key element of this mechanism is that it requires no feedback from the ocean to the atmosphere to effect an increase in variability in the interdecadal time scales. The interdecadal enhancement is also produced even if the atmospheric forcing is spectrally white, i.e., contains equal power at all frequencies. We take advantage of these two characteristics to test whether the stochastic excitation of Rossby waves is setting the time scale seen in ECHO2.

To test for the presence of the Weng and Neelin (1998) mechanism in ECHO2, we make use of the saved surface flux forcing fields, as follows. We first ran just the ocean component of ECHO2 by itself in stand-alone mode, forced by the monthly climatological cycles of heat, momentum, and precipitation minus evaporation ($P-E$) flux saved from the ECHO2 run. Surface relaxation to ECHO2’s climatological SST was imposed in the beginning of this spin-up run, but gradually reduced in strength during the course of the run so that the last 200 years of spin-up were performed with only flux coupling. The entire spin-up was done for 1030 years, at which point the maximum SST drift in the North Pacific was 0.14 K/century, which was deemed sufficiently small for our purposes. Over most of the gyre, the drift was an

order of magnitude less. The final results were detrended at each point to remove the effect of this residual drift.

After the spin-up process, two experiments were performed to determine the applicability of the Weng and Neelin (1998) mechanism to the ECHO2 results. In both experiments, climatological monthly surface fluxes of heat, momentum, and $P-E$ from the ECHO2 run were applied to the ocean model. The experiments were as follows:

1. A control run, imposing the saved ECHO2 monthly surface flux anomalies of heat, momentum, and $P-E$ in the same temporal order as they actually evolved in the ECHO2 run. The point of this run was to see if the technique would yield the same time evolution and interdecadal peak in the power spectra of oceanic variables off Japan as was actually seen in ECHO2. The ability for the stand-alone ocean model to reproduce the ECHO2 results when driven by the saved surface fluxes was considered a requirement for the technique to be useful.

2. A “time permuted” run, where the monthly flux anomalies from the ECHO2 run were applied to the ocean model in random order with replacement, but keeping the proper month number (i.e., a random January field was applied in January, etc.). The applied heat, momentum, and $P-E$ fields were all taken from the same randomly selected source month so they would be self-consistent. The point of this run was to see whether the interdecadal spectral peak would still be present. The mechanism invoking the stochastic excitation of Rossby waves requires only that the applied atmospheric forcing have a large-scale spatial pattern of variability, and have a power spectrum that is statistically white; the time-permutation of the monthly flux anomalies did not change either of those attributes. Therefore, the spectral peak in, for example, SSTA off the coast of Japan should be reproduced in this run if the stochastic excitation mechanism was responsible for the peak. (Note that this also provides an additional check of the Saravanan and McWilliams (1998) mechanism described in the previous section). The time permuted experiment was run for 600 years, almost five times as long as either ECHO2 or the control experiment (137 years). This was done so that the sampling statistics of the time permuted run would be improved.

A comment on the use of monthly flux anomalies to force the ocean model in the time permuted run is warranted. When considering the proper time interval over which to average the surface fluxes before applying them to the ocean model, there is both a minimum and a maximum time interval that could be considered appropriate. At short time intervals, it would be nonsensical to permute the surface fluxes on intervals shorter than the time scale of synoptic midlatitude weather systems (~ 5 days), as doing so would subject the ocean to abrupt changes on time scales generally shorter than are realized in nature. Therefore, the local autocorrelation time scale for weather yields a practical lower limit for the averaging time. At long time scales, averaging over times that are an appreciable fraction of the inter-

decadal time scale of interest here (20 years) would make the results converge to the control run, where the fluxes are not permuted at all. As a compromise, we chose to force the ocean with monthly averaged flux anomalies; this is substantially longer than the time scales associated with midlatitude weather systems, but still far more often than the 20 years/cycle interdecadal time scale we are trying to explain. Note that the ocean model uses a 12-hour time step, which means that a randomly chosen surface forcing is selected once every 360 model time steps. Linear interpolation is used to avoid discontinuities between the selected months’ forcing fields. The separate question of whether the ocean model, when driven by monthly averaged fluxes, can realistically reproduce the behavior it evolves in the fully coupled model is addressed later by analyzing the control run.

This process of taking the surface flux forcing anomalies randomly by month will spectrally whiten the forcing fields at lower frequencies. This is the intended consequence, as we are testing the hypothesis that the interdecadal spectral peak seen in ECHO2 is produced by a mechanism whose forcing has no preferred time scale, but *does* have a preferred spatial structure. But what if the wind stress curl or net surface heat flux forcing in ECHO2 itself had a pronounced interdecadal spectral peak? In such a case any conclusions drawn from the time permuted run, where such a peak would be eliminated by construction, would be meaningless.

To check for this possibility, we did a spectral analysis of yearly averaged wind stress curl and net surface heat flux anomalies from the ECHO2 run at each point over the entire Pacific north of 10°N . We found that the spectra of wind stress curl anomalies are almost uniformly white in ECHO2 over the entire North Pacific basin. The only exceptions are three model gridpoints just south of the Sea of Okhotsk (at locations $49^\circ\text{N}, 149^\circ\text{E}$, $46^\circ\text{N}, 152^\circ\text{E}$ and $46^\circ\text{N}, 155^\circ\text{E}$), which have spectra that are almost flat from 2 to 20 cycles/year, then sharply increase in spectral density to the lowest resolved frequency. It seems implausible that the wind stress curl variability at these few points can cause the 20 year/cycle spectral peak seen in the SAFZ/Kuroshio extension, as the source region is so small and the frequency of spectral enhancement in the source region is lower than 20 years/cycle.

The spectra of the net surface heat flux anomalies are more interesting. In much of the region between the dateline and 120°W the spectra have a distinctly blue character, which, while curious, seems unable to explain an interdecadal spectral peak off Japan. Over most of the rest of the North Pacific the spectra are white. The exception is the SAFZ/Kuroshio extension region itself, where net surface heat flux anomalies *do* have an interdecadal spectral peak (this can be seen in Fig. 10). However, as found in Sect. 3.5.1 when considering the Saravanan and McWilliams (1998) “advective resonance” mechanism, surface heat fluxes in this region act to damp SST anomalies, not generate them. This means that the peak is generated because the driving mecha-

nism for surface heat flux in this region, SST anomalies, itself has a spectral peak, and so the forced response has the same spectral peak. Therefore eliminating this spectral peak might cause low-frequency SST anomalies in the region to be less damped, but will have no effect on the original source of the SST anomalies. Because the applicability of the time-permuted runs to the interpretation of ECHO2 depends on the fact that low-frequency SSTA are atmospherically damped rather than forced in this region, an additional cross-spectral analysis was carried out between SSTA and net surface heat flux there to confirm this relationship (note that only a simple correlation done earlier). It was again found that the low-frequency evolution of SSTA and net surface heat flux is coherent, and at interdecadal frequencies the phase is such that net surface heat flux anomalies damp SST anomalies. We therefore proceed with the interpretation that the time-permuted runs can shed light on the behavior of the ECHO2 model, and in particular on whether the source of the interdecadal spectral peak seen in ECHO2 is a result of the kind of stochastic mechanism described by Weng and Neelin (1998).

The primary result from the control and time permuted runs is shown in Fig. 11. Illustrated are the spectra of SSTA averaged over the Kuroshio extension region off Japan for ECHO2, the control run, and the time-permuted run. Processing is as in Fig. 10, in particular, the spectra are pre-whitened to remove the AR(1) component, which is not of primary interest here. The spectra for the fully coupled run (ECHO2) and for the control run both show the spectral peak at the previously-identified period of ~ 20 years/cycle. A cross-spectral analysis (not shown) between the raw SST time series for these two runs in the SAFZ region shows a squared coherence between 0.5 and 0.6 for frequencies between 5 and 25 years/cycle (the 95% significance level is 0.2). The phase is not discernibly different from zero at

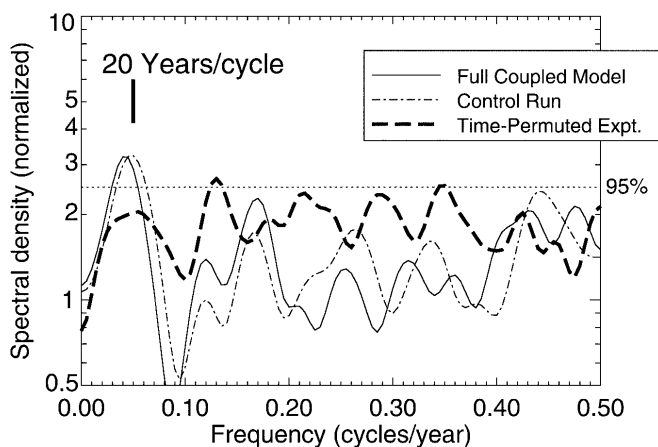


Fig. 11 Spectra of SSTA in the Kuroshio region off Japan (150°E , 40°N) for the ECHO2 run (*thin solid*), control run forced by ECHO2 fluxes taken sequentially (*thin dash-dot*), and test run with monthly ECHO2 fluxes taken in random time order (*thick dash-dot*). The 95% significance level is indicated by the *dotted line*

any frequency where the coherence is significant. Thus, the control run effectively reproduces the low-frequency time evolution of SSTA found in the ECHO2 run, and we conclude from this that the technique is practicable. The time permuted run (thick dashed line of Fig. 11) lacks the interdecadal spectral peak seen in the other two runs. This suggests that the Weng and Neelin (1998) effect is *not* the source of the interdecadal spectral peak seen in the ECHO2 run. Another way of interpreting this result is that the spectrum seen in the time permuted run is an estimate of the size of the Weng and Neelin effect in this particular model, and that the actual interdecadal peak seen in ECHO2 significantly exceeds this size, and so must be due to additional causes.

The conclusion to be drawn from the control and time permuted runs shown here is that the ~ 20 year/cycle spectral peak seen in ECHO2 is *not* due to the stochastic excitation of Rossby waves by atmospheric forcing of a preferred spatial pattern. This does not constitute evidence that such a process does not occur in the model, but rather that most of the variance in the specific spectral peak seen in oceanic variables off the coast of Japan in ECHO2 is generated by other effects. Furthermore, the fact that the control run reproduces the spectral peak while the time permuted run does not is evidence that a coupled ocean/atmosphere phenomenon must be responsible for the spectral peak. When either the fully coupled run (ECHO2) or the control experiment evolve forward in time, oceanic and atmospheric processes conspire to produce a significant spectral peak in SSTA off Japan. However, when the time order of the forcing is changed, destroying any synchronicity between the atmosphere and ocean on time scales longer than one month, the same ocean model does not produce any such peak. The low-frequency evolution of the atmosphere and ocean must be synchronized to explain these results. Even more, it is not sufficient for the ocean merely to respond to the low-frequency evolution of the atmosphere to produce the spectral peak; this happens in the time permuted case, yet no peak is seen. It must be that the atmosphere is also responding to the ocean on low frequencies, and that both these effects are needed to properly reproduce the low-frequency evolution of the North Pacific.

3.5.3 Dynamical coupling via the wind stress curl

Latif and Barnett (1994, 1996) suggested that a dynamical feedback between the midlatitude ocean and atmosphere might produce North Pacific climate variability as follows. A strengthened subtropical gyre circulation in the Pacific brings more warm water northwards into the Kuroshio extension region, decreasing the meridional temperature gradient across the subtropical gyre. The normally negative wind stress curl ($\nabla \times \tau$) over the subtropical gyre decreases in strength in response to the decrease in meridional temperature gradient, i.e., increases numerically (a positive anomaly).

The positive $\nabla \times \tau$ anomaly tends to spin down the gyre, resulting in less warm water advected northwards into the Kuroshio extension region, completing a half cycle.

The evidence from the control and “permuted time” runs presented in the previous section supports the idea that a coupled ocean/atmosphere feedback produces the interdecadal spectral peak seen in SSTA off Japan in ECHO2. Therefore, we test here the idea that the Latif and Barnett (1994) mechanism is giving rise to this variability. To do this we will examine whether several critical pieces of this chain of events are present in the ECHO2 run: (1) a positive anomaly in the central Pacific $\nabla \times \tau$ leading to cold SSTAs off Japan, with a time lag of several years; (2) cold SSTAs off Japan spreading into the central Pacific enough to be able to influence the overlying atmosphere; (3) changes in SSTA (or gradients thereof) effecting changes in central Pacific $\nabla \times \tau$ of the required sign. Of the three, the third is the most uncertain; there is every reason to think that changes in $\nabla \times \tau$ are reflected in changes in transport of the western boundary current (although the time lag and effect on temperature needs to be established), and that advective transport of temperature anomalies by the Kuroshio should exist, but various studies have found conflicting results on what effect midlatitude SSTAs have on the overlying atmosphere (e.g., Palmer and Sun 1985; Kushnir and Lau 1992; Graham et al. 1994; Kushnir and Held 1996). An attempt to understand the source of these differences will be made later.

When considering the possibility that a change in wind stress curl over the central Pacific can have delayed temperature repercussions along the western boundary, Venzke et al. (2000b) showed that Rossby wave propagation in HOPE (the oceanic component of the ECHO2 coupled model examined here) does indeed carry information about wind stress curl changes in the central gyre westwards to the boundary, as required by the Latif-Barnett mechanism. Rather than repeating that analysis here, we will show a straightforward lagged correlation between changes in SSTA over the region 35–45°N, 140–160°E (in the SAFZ/Kuroshio extension region) and preceding changes in $\nabla \times \tau$ over the rest of the Pacific. The results are in Fig. 12, which shows the spatial correlation field at leads of three, four, and five years (top, middle, and bottom panels, respectively) with changes in $\nabla \times \tau$ leading changes in SSTA. The data have been bandpass filtered to retain only periods between 10 and 40 years/cycle, in keeping with our interest in interdecadal time scales.

At a lead of three years, a negative correlation is seen over almost the entire Pacific between 30°N and 50°N; the negative sign arises because positive wind stress curl anomalies are associated with (delayed) decreases in SST. The location of the maximum negative correlations is close to the latitude of boundary between the subpolar and subtropical gyres. This suggests that a response could potentially participate equally in both gyres, or simply be reflected in a latitudinal shift of the boundary between them. At longer leads, the region of maximum

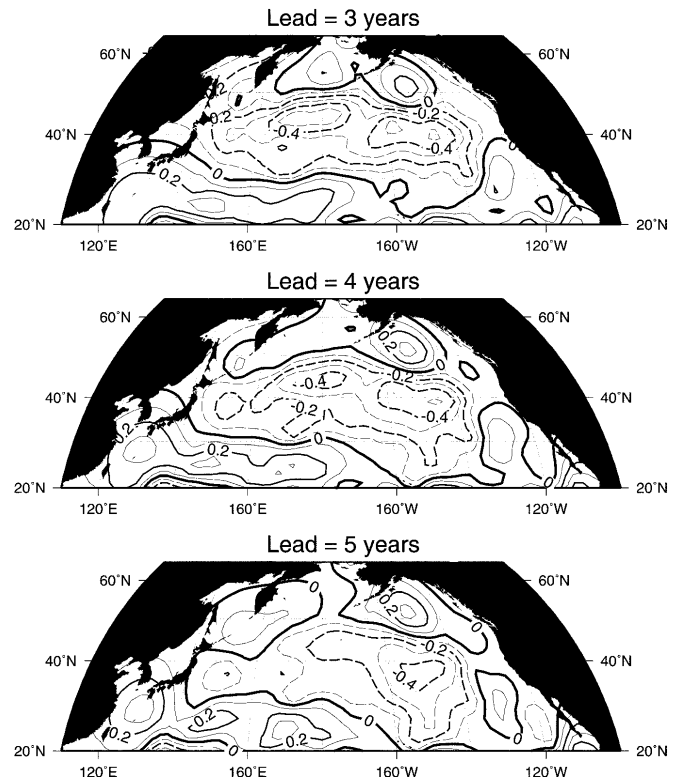


Fig. 12 Lagged correlation between changes in wind stress curl over the Pacific basin and changes in SSTA off Japan. *Top*: wind stress curl leading SSTA by three years. *Middle*: by four years. *Bottom*: by five years

negative correlation moves south and east. The peak value drops from -0.59 at a lead of three years to -0.45 at a lead of five years, and fades to -0.35 at a lead of eight years. These values are not particularly large; the yearly wind stress curl anomalies in ECHO2 generally have a white spectrum in the North Pacific, so a reasonable estimate of the degrees of freedom for the 10-year filtered wind stress curl data is 14 (given the run length of 137 years). This indicates that the 95% significance level for the correlation is about 0.45, which is exceeded only in limited areas between 35°N and 45°N. Note that the quality of the correlation may be degraded somewhat because the plotted fields are numerically calculated derivatives in time (and the wind stress curl is a numerically calculated derivative in space as well), which tends to add noise.

A lagged correlation between observed (da Silva et al. 1995) SSTA off Japan and wind stress curl over the Pacific basin over the period 1965 to 1993, using 10-year low-pass filtered data, shows a noisy but similar pattern, with negative values north of 33°N (not shown). The time scale is shorter than is found in the model, with peak correlations < -0.8 between 175°E and 165°W at a lead of two years, and fading after that. Deser et al. (1999), in an analysis of North Pacific observations covering the 1970s and 1980s, found that decadal-time scale changes in basin-wide wind stress curl lead changes in western boundary thermocline depth (between 30°N

and 40°N) by 4–5 years. Although we are concerned here with changes in western boundary SST rather than thermocline depth, the agreement in time scale nevertheless supports the idea that the time scale obtained from the model is reasonable.

This analysis shows that changes in wind stress curl lead changes in SSTA off Japan in the sense required by the Latif–Barnett mechanism, but it also indicates that the delay is no more than three to five years for a half cycle, too short to explain a 20 year/cycle oscillation. A similar analysis using the lagged correlation between SSTA and $\nabla \times \tau$ (rather than the *changes* in SSTA and $\nabla \times \tau$ used above) finds the same time delay. Can this mechanism, then, be responsible for a twenty year time scale? Another important part of the path not considered yet, and that would be expected to introduce an additional delay, is that from SSTAs just off Japan to SSTAs spread over enough of the North Pacific to have an influence on the overlying atmosphere. (Note that the necessity of this step is unproven; it has also been argued that the region immediately off Japan is the only relevant location for influencing the atmosphere, since surface heat loss to the atmosphere is concentrated there, (Arthur Miller, personal communication). Such a mechanism would require processes different from those considered here to explain the 20 year time scale.

Figure 13 shows, via a lagged correlation, the propagation of signals off Japan into the central North Pacific. Rather than straight SSTA, ∇^2 SSTA is shown because of the importance of SST gradients in exerting torque on the atmosphere, thereby effecting changes in

the wind stress curl (Barnett and White 1972). ∇^2 SSTA tends to have a white spectrum in the region between 160°E and 160°W, so taking 14 degrees of freedom for the filtered data indicates that a correlation of about 0.45 would be significant at the 95% level. Areas with this correlation or greater are shaded in the figure. In addition to the oscillating signal with a time scale of about 20 years/cycle previously identified from the spectral analysis, Fig. 13 demonstrates that there is a delay of ~ 5 years for a signal to propagate from the region immediately off Japan to the dateline. Added to the three to five year delay between changes in wind stress curl to changes in SSTA off Japan, this leads to a time scale of eight to ten years for a half cycle, in reasonable agreement with the frequency of ~ 20 years/cycle identified from the spectral analysis. (It is assumed that any atmospheric response to changes in central Pacific ∇^2 SSTA do not require an appreciable time lag to get set up.)

Figure 14 shows a similar plot made from observed SSTA along 41°N over the years 1945–1993 (da Silva et al. 1995). The results are noisy, but do show a multi-year propagation of ∇^2 SSTA from the region off Japan into the central Pacific. The propagation time is slower than that seen in the model, closer to 10 years to go from the extreme west to the dateline, rather than the five years seen in the model, which suggests that a real-world analog of this oscillation might be shifted to somewhat lower frequencies than found in the models. With the few degrees of freedom, none of the values is statistically significant, which leaves the applicability of this propagation in the real world open to question. (Note, though, that this plot is constructed by numerically calculating

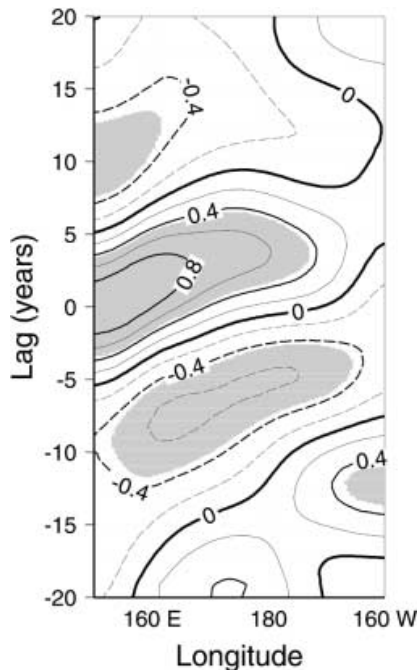


Fig. 13 Lagged correlation between ∇^2 SSTA at 40°N, 155°E and in a line along 40°N from the ECHO2 coupled model. The sense of the lag is such that signals at 155°E lead those in near the dateline by about five years. Shaded regions are significant at the 95% level

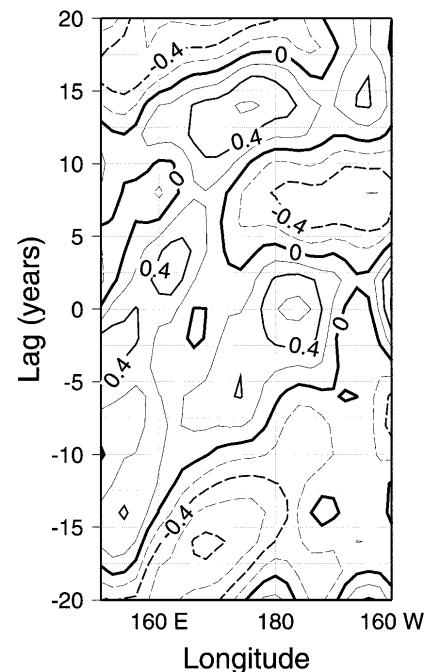


Fig. 14 As in Fig. 13, but for observations over the period 1945–1993

the second derivative of the observed SST field in latitude and longitude, a process that generates noise.)

The last piece of the Latif–Barnett mechanism to examine is the response of the atmosphere to an imposed midlatitude SSTA. To test whether this can have the effect on wind stress curl predicted by the Latif–Barnett mechanism, we ran an experiment with SSTAs imposed as lower boundary conditions to ECHAM4, the atmospheric model used in ECHO2. The SST anomalies are imposed in two phases: by adding the anomaly pattern to climatological SSTs at all months (the positive phase) and by subtracting it from climatological SSTs at all months (the negative phase). Note in particular that these are *not* “perpetual January”-type simulations such as used in Latif and Barnett (1994, 1996), but rather full-year runs. The motivation for doing the experiments this way is that Peng et al. (1997) found that the atmosphere’s response to midlatitude SST anomalies can vary substantially by month; since we find an interdecadal spectral peak, the mechanism causing it can be presumed to be active over time scales of many months. Therefore, whole-year experiments are used to average the effects of the SST anomaly on the atmosphere over the entire seasonal cycle. This avoids any errors arising from an unusually strong model response coincidentally occurring in January. The positive and negative phases were each run for 12 years, for a total of 288 months.

The SSTA pattern used to force the model is shown in Fig. 15. Values were linearly ramped to zero starting at 22°N and ending at 15°N, so that there are no SSTAs south of 15°N. This was done so that the teleconnected effect of SSTAs in the tropical wave guide would be excluded from the results. The pattern itself is taken from the leading EOF of 10–40 year bandpassed SSTA of ECHO2. This is an important point, because this means that we are testing the model response to a pattern that is self-consistent with the model’s own variability. Previous work has shown that latitudinal shifts in the location of a midlatitude SST anomaly can have a strong effect on the atmosphere’s response (Peng et al. 1997). Thus, it is important to draw conclusions about the atmosphere’s response to a midlatitude SSTA only from experiments where the anomaly is imposed in a location consistent with the model’s own variability,

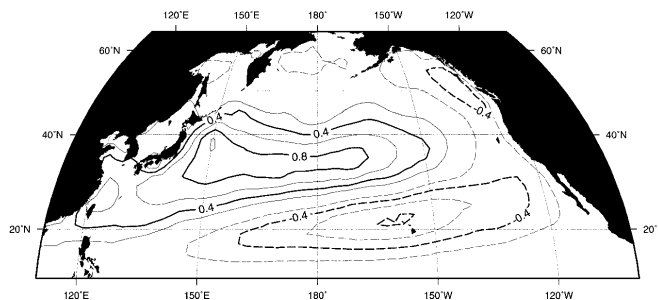


Fig. 15 Pattern of SST anomaly imposed as a lower boundary condition on the atmospheric test runs. Contour level is 0.2 K

rather than some arbitrary placement. The strength of the pattern, with a maximum of 1 K, is overstated relative to the size of observed SSTA fluctuations in the North Pacific, which have a standard deviation of about 0.4 K.

The results from the SSTA-forced experiment are shown for 500 mb geopotential height anomaly in Fig. 16. Plotted is the difference between the average of the 144 positive phase months and the 144 negative phase months. Shaded areas show where a response is found at greater than 95% significance level using a *t*-test, taking the number of degrees of freedom to be 12 (i.e., each year is treated as an independent sample). There is a downstream high pressure anomaly of 15 gpm over the central North Pacific, and a low of 30 gpm over northwest North America.

Barnett et al. (1999b) previously showed that the $\nabla \times \tau$ field does, indeed, respond to midlatitude SST anomalies in the sense required by the Latif–Barnett mechanism. This was shown by making use of a particular $\nabla \times \tau$ pattern they termed $\hat{\tau}$, which was found by linear regression to be associated with the model’s interdecadal variability. The purpose of introducing $\hat{\tau}$ was to emphasize that the atmosphere’s response has projection onto the wind stress pattern associated with the interdecadal variability. Rather than repeating that analysis here, we will simply show the difference in $\nabla \times \tau$ between the positive and negative phases of imposed SST anomaly. This is a complementary presentation of the results in the sense that it is a more direct illustration of the atmosphere’s response, but less specifically targeted towards the interdecadal variability, and so might be distorted by effects unrelated to the oscillation we are interested in.

The effect of the imposed SSTA on the $\nabla \times \tau$ field is shown in Fig. 17 as simply the difference between the time-averaged positive and negative phase runs. Shaded areas show where a response is found at greater than 95% significance level using a *t*-test, taking the number of degrees of freedom to be 12 (i.e., each year treated as an independent sample). In the central/west Pacific, there is a broad area of positive $\nabla \times \tau$ response between 30°N and 50°N, extending to 60°N in the central Pacific.

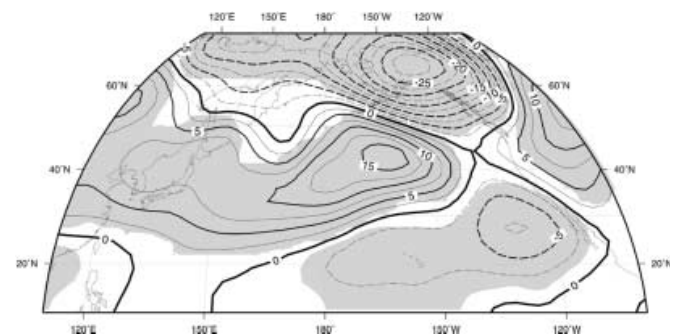


Fig. 16 Difference in 500 mb geopotential height between the experiment with imposed positive and negative SSTA as a lower boundary condition. Shaded areas are significant at the 95% level

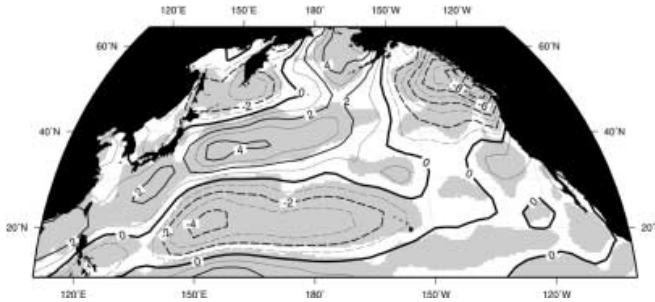


Fig. 17 Difference in wind stress curl response between the experiments with the positive and negative phase of SST anomalies imposed beneath the ECHAM4 atmospheric model. Results are averaged over the entire run (288 months total). Contour level is 1.0×10^{-8} Pa/m. Shaded areas show where the difference is significant at the 95% level

Values of the wind stress curl response are $2\text{--}4 \times 10^{-8}$ Pa/m; by comparison, climatological values of monthly-averaged wind stress curl in the region are in the range of $7\text{--}10 \times 10^{-8}$ Pa/m. Thus, the response is easily strong enough to have an important influence on the ocean's circulation, even taking into account the fact that the imposed SSTA was larger than observed. Compared to the results in Latif and Barnett (1994, 1996), who used ECHAM3 and found a positive wind stress curl response over approximately $20\text{--}40^\circ\text{N}$, the response found here with ECHAM4 is shifted about 10° to the north ($30\text{--}50^\circ\text{N}$). The positive response is approximately centered on the latitude of the boundary between the subpolar and subtropical gyres, suggesting that the response could be felt in either of the gyres or simply reflected as a latitudinal shift in the boundary between the two. Such a shift would be expected to accompany large SST anomalies, since this is where the largest meridional temperature gradients exist. The location of $\nabla \times \tau$ response is consistent with the relationship between lagged changes in wind stress curl and SST off Japan shown in Fig. 12; note that the positive region shown in Fig. 17 is largely coincident with the region of negative lagged correlation shown in Fig. 12. It is also near the latitude of the propagating $\nabla^2\text{SST}$ anomaly, which is seen around 40°N . It is possible that the region of negative wind stress curl response reaching down to 10°N , a feature not seen in Latif and Barnett (1994, 1996), might have implications for circulation in the tropical regions, but this will not be explored further here.

In sum, the results from the ECHO2 model show that the necessary pieces are present to explain the interdecadal spectral peak by a dynamical ocean/atmosphere feedback. This can be accomplished via the demonstrated sensitivity of the atmosphere's wind stress curl field to sea surface temperature anomalies. The 20-year time scale is understandable given the proviso that large-scale changes in the atmosphere's wind stress curl pattern require spreading of $\nabla^2\text{SST}$ anomalies from the immediate vicinity of the western boundary region into an appreciable fraction of the central North Pacific. Note that the results shown here are a consistency check,

not a proof of the dynamical origins of the ~ 20 year/cycle spectral peak. The correlations found are statistically significant but not strongly so. The overall picture is that the extra enhancement of variance at the ~ 20 year/cycle time scale that reaches above the background AR(1) spectrum is consistent with a dynamical ocean/atmosphere feedback mechanism. In ECHO2's Kuroshio extension region, about 56% of the overall enhancement in interdecadal spectral power due to ocean dynamics was accounted for by a strengthening of the AR(1) spectrum, and 44% by departures from this that could be due to a coupled mode.

4 Discussion

The results of the previous section show that variability in the North Pacific has two components, a North Pacific mode and a dynamic western Pacific mode. These are distinguished by their spatial distribution and spectral structure.

The signature of the North Pacific mode is found over the entire central Pacific north of 20°N , and has a spectrum that is not significantly different from an AR(1) process. This mode has previously been identified from observations by Deser and Blackmon (1995) and Zhang et al. (1996), and, by their linear statistical analyses, suggested to be independent of ENSO. The fact that numerical models that lack ENSO still have the North Pacific mode (as can be seen in Fig. 1) provides strong confirmation of this in a framework where the influence of (possibly nonlinear) atmospheric dynamics are taken into account.

The models used to reach this conclusion lack ENSO, but still have some degree of tropical SST variability, albeit with reduced variance and no spectral peaks in the 2–7 year ENSO band. Can the North Pacific mode, then, be a teleconnected response to *non*-ENSO tropical variability? The results shown in Sect. 3.1 argue against this. To see this, assume for the moment that the North Pacific mode *is* a teleconnected response to tropical SST variability not related to ENSO. There are three possibilities: (a) the spectrum of hypothesized tropical forcing might have power only in the ENSO frequency band; (b) it might have power only outside the ENSO band; (c) it might have power both in and outside the ENSO band. The results show that the amplitude of the North Pacific mode in the models without ENSO is realistic, with values of 0.3–0.6 K versus the observed value of 0.4 K; in the ECHO2 coupled model, which includes ocean dynamics and has a realistically strong ENSO, the amplitude of the North Pacific mode is 0.5 K, again close to the observed value. Since the strength of the ENSO-frequency forcing changes greatly between these runs with little change in the North Pacific mode, possibilities (a) and (c) are implausible. Yet the spectra of the North Pacific mode shown in Fig. 1 do *not* have power only outside the ENSO band, but rather are indistinguishable from an ordinary AR(1) processes; the spectrum from

ECHO2 (not shown) shows the same. Thus possibility (b) seems unlikely. Hence we conclude that the North Pacific mode is not a teleconnected response to tropical SST anomalies, be they of ENSO origin or otherwise. We might loosely sum this up by saying that if a response stays the same while a conjectured forcing varies strongly, the conjectured forcing cannot be the source of the response after all. Note that it is a separate question, not addressed here, whether the phase of the North Pacific mode and ENSO are somehow related by physical interactions.

Another question is whether the North Pacific mode itself has remote repercussions in the tropics. It was suggested that this might be the case on the basis of statistical analysis of models and observations by Pierce et al. (2000) and Barnett et al. (1999a), where it was shown that the North Pacific mode is associated with changes in surface wind stress anomaly that reach into the tropics, thereby having an effect on ENSO. The work here completes that picture by demonstrating in a dynamically self-consistent way that, indeed, the North Pacific mode is *not* a teleconnected response to tropical SST variability. Thus, the direction of causality for wind stress associated with the North Pacific mode must be from the North Pacific to the tropics, rather than the other way around. The details of a mechanism that could accomplish this remain to be explored, but we note that the link between the North Pacific mode and cloudiness demonstrated in Sect. 3.3 suggests that evolution of the North Pacific mode is associated with modest but consistent changes in the large-scale circulation of the atmosphere over at least the region north of 10°N. These changes in cloudiness associated with the North Pacific mode can be seen in the mixed layer runs that lack ENSO, the full coupled ocean/atmosphere model ECHO2, and in the observations.

The dynamic western Pacific mode of variability has a statistically significant spectral peak at about 20 years/cycle, and in the models is preferentially found in the SAFZ/Kuroshio extension region of the western Pacific. The analysis of Sect. 3.5 suggests that the source of this peak is a coupled ocean/atmosphere interaction, rather than a one-way response of the ocean to stochastic atmospheric forcing. We have shown in Sect 3.5.3 the results of checking that the source of this peak is the dynamical mechanism proposed by Latif and Barnett (1994, 1996). The critical pieces of this mechanism are present in the model, and have the proper overall delay to account for the 20year/cycle spectral peak. An important note to the determination of the time scale is that the mechanism requires that the delay for anomalies to propagate from the extreme western Pacific into the central Pacific be added into the overall delay if the 20 year time scale is to be accounted for. Such a propagation can be seen in both the model (Fig. 13) and observations (Fig. 14).

One point not addressed here, but which should be kept in mind as an open question and future area of research, is what connection there might be between the

North Pacific mode and the dynamic western Pacific mode. The observations suggest that the enhancement of low-frequency variability in nature is not as confined to the western boundary as found in the models. It is reasonable to suppose that the models, with their relatively coarse resolution in the midlatitudes (typically $\sim 2.8^\circ$) do not represent the advective processes associated with the Kuroshio current with a high degree of fidelity. This might serve to keep artificially separated modes that, in nature, have a stronger interaction. Detailed, Pacific-wide observations of such variables as SST, surface wind stress, cloudiness, and surface heat flux would be required over a century or two to address this conclusively from observations. In lieu of such a data set, a reasonable way to proceed would be with coupled numerical models that have fine enough grid spacing to resolve the western boundary currents in the North Pacific and the dynamical processes in Kuroshio extension region.

5 Conclusions

Our goal in this work was to attribute various aspects of North Pacific climate variability to one of three mechanisms: (1) the ocean's thermodynamic response to the atmosphere's stochastic heat flux forcing; (2) the ocean's dynamic response to the atmosphere's stochastic heat flux and wind stress forcing, with no feedback to the atmosphere; (3) fully coupled, dynamical ocean/atmosphere interactions. Our particular emphasis is on the third mechanism, as this would be potentially predictable by coupled ocean/atmosphere general circulation models.

We have examined this question by using the output of a variety of coupled and stand-alone ocean and atmosphere models, as well as from observations as available. The intent of using multiple models is to draw conclusions from features they have in common; nevertheless, numerical models have their own set of limitations and ways in which they systematically misrepresent reality, which must be kept in mind. On the other hand, a difficulty with using the observations is that we are primarily interested in variability on inter-decadal time scales, which is problematic given the relatively short observed record over the Pacific. We have tried to appropriately combine the two approaches in reaching the following conclusions.

1. The characteristic spatial pattern of the "North Pacific mode" (Deser and Blackmon 1995) is primarily set by stochastic atmospheric heat flux forcing thermodynamically integrated in situ by the ocean's mixed layer. Latent heat flux is the main forcing term determining this pattern, with typical values of 20–30 W/m² for one standard deviation of the North Pacific mode time series. Also important is the divergence of the Ekman transport by the anomalous wind stress associated with the mode, which contributes 10–20 W/m² of surface forcing, and changes in solar forcing that accompany changes in fractional cloudiness on the order

of 3–5% over the central Pacific between 10 °N and 40 °N, which also contribute 10–20 W/m². Such changes in cloudiness are seen in the observations as well as the models. Sensible and longwave forcing of the North Pacific mode are negligible. The model setup does not allow an evaluation of the role of vertical mixing across the base of the mixed layer.

2. The North Pacific mode is not just a teleconnected response to ENSO processes. Even in models that lack ENSO, it appears with its characteristic shape and an amplitude of 0.3–0.6 K, compared to 0.4 K from the observations. The spectrum of the North Pacific mode cannot be distinguished from that of an AR(1) process in either the models or observations over the period 1945–1999.

3. Ocean dynamics act to increase SST variability in the subarctic frontal zone (SAFZ)/Kuroshio extension region of the North Pacific by an order of magnitude. The observations suggest that there is also a region of enhanced interdecadal variability along the west coast of North America, but for unknown reasons the models do not reproduce this.

4. The majority of the low-frequency enhancement in SST variability in the SAFZ/Kuroshio extension region arises from a process with an AR(1) spectrum. Superimposed on this red-noise background is a spectral peak at a time scale of about 20 years/cycle. Numerical experiments show that this additional interdecadal enhancement in SST variability arises from coupled ocean/atmosphere interactions. Analysis of the model results shows that this coupled interaction is consistent with the suggestion of Latif and Barnett (1994, 1996) that it is accomplished via a sensitivity of the wind stress curl field over the North Pacific to midlatitude SST anomalies. The time scale of the oscillation is set by the 3–5 year delay (per half cycle) imposed by the lagged response of western boundary SSTs to changes in central Pacific wind stress curl changes, plus another five year delay for the signal to spread from the extreme western Pacific off Japan out into the central Pacific (and subsequently influence the atmosphere). Similar time lags are found in the observations as well, with somewhat shorter (2–4 year) lags from changes in wind stress curl to western boundary SSTs, but somewhat longer (6–8 year) lags for signals to propagate from the extreme western to central Pacific.

Work that remains to be done in this area is: (a) a more direct check of the Latif–Barnett mechanism, for example by disabling the physics necessary for the feedback and redoing the long coupled model run to ensure that the spectral peak is eliminated; (b) determining what interaction, if any, there is between the North Pacific mode (which is primarily in the central North Pacific, and largely stochastically forced by the atmosphere with only ocean thermodynamics being important) and the coupled, dynamic mode (mostly in the western Pacific, and largely dependent on a coupled ocean/atmosphere interaction for setting its characteristic time scale). The observations suggest that the

interdecadal variability is trapped too far west in the models, which may have the effect of keeping the modes unrealistically separated. It is reasonable to suppose that models with finer resolution in the critical western boundary and Kuroshio extension regions are necessary to make progress on this question.

Acknowledgements This work benefited from discussions with Arthur Miller of Scripps, which we gratefully acknowledge. This work was supported by the Department of Energy's CCpp Program (DE-FG03-91-ER61215), NSF Grant OCE97-11265, the Scripps Institution of Oceanography, and the German government under its Decadal Predictability grant. The simulations were executed at NCAR's Scientific Computing Division (SCD) and Climate Simulation Laboratory (CSL), supplemented with runs at the National Energy Research Scientific Computing Center (NERSC). We thank Lennart Bengtsson and Erich Roeckner for allowing us to use the ECHAM4 atmospheric model.

References

- Arakawa A, Lamb VR (1977) Computational design of the basic dynamical processes of the UCLA general circulation model. *Meth Comput Phys* 17: 173–265
- Barnett TP, White WB (1972) A servomechanism in the ocean/atmosphere system of the mid-latitude North Pacific. *J Phys Oceanogr* 2: 372–381
- Barnett TP, Preisendorfer R (1988) Origins and levels of monthly and seasonal forecast skill for United States surface air temperatures determined by canonical correlation analysis. *Mon Weather Rev* 115: 1825–1850
- Barnett TP, Latif M, Graham N, Flugel M, Pazan S, White W (1993) ENSO and ENSO-related predictability. Part I: predictions of equatorial Pacific sea surface temperature with a hybrid coupled ocean/atmosphere model. *J Clim* 6: 1545–1566
- Barnett TP, Pierce DW, Latif M, Dommenges D, Saravanan R (1999a) Interdecadal interactions between the tropics and midlatitudes in the Pacific basin. *Geophys Res Lett* 26: 615–618
- Barnett TP, Pierce DW, Saravanan R, Schneider N, Dommenges D, Latif M (1999b) Origins of the midlatitude Pacific decadal variability. *Geophys Res Lett* 26: 1453–1456
- Barsugli J, Battisti DS (1998) The basic effects of atmosphere–ocean thermal coupling on midlatitude variability. *J Atmos Sci* 55: 477–493
- Blackmon ML, Geisler JE, Pitcher EJ (1983) A general circulation model study of January climate anomaly patterns associated with interannual variation of equatorial Pacific sea surface temperatures. *J Atmos Sci* 40: 1410–1425
- Boville BA, Gent PR (1998) The NCAR Climate System Model, Version One. *J Clim* 11: 1115–1130
- da Silva AM, Young CC, Levitus S (1995) Atlas of surface marine data 1994, vol 1: algorithms and procedures. “Technical Report”, Available from NOAA Atlas NESDIS 6, US Department Commerce
- Deser C, Blackmon ML (1995) On the relationship between tropical and North Pacific sea surface temperature variations. *J Clim* 8: 1677–1680
- Deser C, Alexander MA, Timlin MS (1999) Evidence for a wind-driven intensification of the Kuroshio current extension from the 1970s to the 1980s. *J Clim* 12: 1697–1706
- DKRZ (1992) The ECHAM3 Atmospheric General Circulation Model. Technical Report “Technical Report 6”, Available from Deutsches Klimarechenzentrum, Hamburg, Germany
- Frankignoul C, Hasselmann K (1977) Stochastic climate models. Part II: application to sea-surface temperature anomalies and thermocline variability. *Tellus* 29: 284–305
- Frankignoul C (1985) Sea surface temperature anomalies, planetary waves, and air-sea feedback in the middle latitudes. *Rev Geophys* 23: 357–390

- Frankignoul C, Muller P, Zorita E (1997) A simple model of the decadal response of the ocean to stochastic wind forcing. *J Phys Oceanogr* 27: 1533–1546
- Frey H, Latif M, Stockdale T (1997) The coupled GCM ECHO-2, Part I: the tropical Pacific. *Mon Weather Rev* 125: 703–720
- Gent PR, McWilliams JC (1990) Isopycnal mixing on ocean circulation models. *J Phys Oceanogr* 20: 150–155
- Gershunov A, Barnett TP (1998) Interdecadal modulation of ENSO teleconnections. *Bull Am Meteorol Soc* 79: 2715–2725
- Graham NE, Barnett TP, Wilde R, Ponater M, Schubert S (1994) On the roles of tropical and midlatitude SSTs in forcing interannual to interdecadal variability in the winter northern hemisphere circulation. *J Clim* 7: 1416–1441
- Hasselmann K (1976) Stochastic climate models. I. Theory *Tellus* 28: 473–485
- Holland WR, Chow JJ, Bryan FO (1998) Application of a third-order upwind scheme in the NCAR ocean model. *J Clim* 11: 1487–1493
- Horel JD, Wallace JM (1981) Planetary-scale atmospheric phenomena associated with the Southern Oscillation. *Mon Weather Rev* 109: 813–829
- Jin FF (1997) A theory of interdecadal climate variability of the North Pacific ocean/atmosphere system. *J Clim* 10: 1821–1835
- Kiehl JT, Hack JJ, Bonan GB, Boville BA, Briegleb BP, Williamson DL, Rasch PJ (1996) Description of the NCAR Community Climate Model (CCM3). Technical Report “NCAR Technical Note TN-420”. Available from National Center for Atmospheric Research, Boulder, CO, USA
- Kushnir Y, Lau NC (1992) The general circulation model response in a North Pacific SST anomaly; dependence on time scale and pattern polarity. *J Clim* 5: 271–283
- Kushnir Y, Held IM (1996) Equilibrium atmospheric response to North Atlantic SST anomalies. *J Clim* 9: 1208–1219
- Large WG, McWilliams JC, Doney SC (1994) Oceanic vertical mixing: a review and a model with a nonlocal boundary layer parameterization. *Rev Geophys* 32: 363–403
- Latif M, Stockdale T, Wolff J, Burgers G, Maier-Reimer E, Junge M, Arpe K, Bengtsson L (1994) Climatology and variability in the ECHO coupled GCM. *Tellus* 46: 351–366
- Latif M, Barnett TP (1994) Causes of decadal climate variability over the North Pacific and North America. *Science* 266: 634–637
- Latif M, Barnett TP (1996) Decadal climate variability over the North Pacific and North America: dynamics and predictability. *J Clim* 9: 2407–2423
- Levitus S (1994) World ocean atlas 1994. “Technical Report”, Available from US Department of Commerce, National Oceanic and Atmospheric Administration, USA
- Manabe S, Stouffer RJ (1996) Low-frequency variability of surface air temperature in a 1000-year integration of a coupled atmosphere-ocean-land surface model. *J Clim* 9: 376–393
- Mantua NJ, Hare SR, Zhang Y, Wallace JM, Francis RC (1997) A Pacific interdecadal climate oscillation with impacts on salmon production. *Bull Am Meteorol Soc* 78: 1069–1079
- Miller AJ, Cayan DR, Barnett TP, Graham NE, Oberhuber JM (1994) Interdecadal variability of the Pacific Ocean: model response to observed heat flux and wind stress anomalies. *Clim Dyn* 9: 287–302
- Munnich M, Latif M, Venzke S, Maier-Reimer E (1998) Decadal oscillations in a simple coupled model. *J Clim* 11: 3309–3319
- NCAR (1997) The NCAR CSM Ocean Model Technical Note. Technical Report “Technical Note NCAR/TN-423”, Available from National Center for Atmospheric Research, Boulder, CO, USA
- Pacanowski R, Dixon K, Rosati A (1993) The G.F.D.L. Modular Ocean Model Users Guide. GFDL Ocean Group Technical Report 2
- Palmer TN, Sun Z (1985) A modelling and observational study of the relationship between sea surface temperature in the north-west Atlantic and the atmospheric general circulation. *Q J R Meteorol Soc* 111: 947–975
- Peng S, Robinson WA, Hoerling MP (1997) The modeled atmospheric response to midlatitude SST anomalies and its dependence on background circulation states. *J Clim* 10: 971–987
- Pierce DW, Barnett TP, Latif M (2000) Connections between the Pacific Ocean tropics and midlatitudes on decadal time scales. *J Clim* 13: 1173–1194
- Robertson AW (1996) Interdecadal variability over the North Pacific in a multi-century climate simulation. *Clim Dyn* 12: 227–241
- Roeckner E, Arpe K, Bengtsson L, Dumenil L, Kirk E, Lunkeit F, Ponater M, Rockel B, Sausen R, others (1992) Simulation of the present day climate with the ECHAM model: impact of model physics and resolution. Technical Report “Report 93”, Available from MPI fur Meteorologie, Bundesstr. 55, 20146 Hamburg, Germany
- Roeckner E, Arpe K, Bengtsson L, Christoph M, Claussen M, Dumenil L, Esch M, Giorgetta M, Schlese U, Schulzweida U (1996) The Atmospheric General Circulation Model ECHAM-4: model description and simulation of present-day climate. Technical Report 218, available from DKRZ, Bundesstr. 55, 20146, Hamburg, Germany
- Saravanan R, McWilliams JC (1998) Advective ocean/atmosphere interactions: an analytical stochastic model with implications for decadal variability. *J Clim* 11: 165–188
- Trenberth KE, Hurrell JW (1994) Decadal atmosphere-ocean variations in the Pacific. *Clim Dyn* 9: 303–319
- Venzke S, Latif M, Villwock A (2000a) The Coupled GCM ECHO-2. Part II: Indian Ocean response to ENSO. *J Clim* 13: 1371–1383
- Venzke S, Munnich M, Latif M (2000b) On the predictability of decadal changes in the North Pacific. *Clim Dyn* 16: 379–392
- Weng WJ, Neelin JD (1998) On the role of ocean-atmosphere interaction in midlatitude interdecadal variability. *Geophys Res Lett* 25: 167–170
- Wolff J-O, Maier-Reimer E, Legutke S (1997) HOPE, The Hamburg Ocean Primitive Equation Model. Technical Report available from DKRZ, Bundesstr. 55, 20146, Hamburg, Germany
- Zhang Y, Wallace JM, Iwasaka N (1996) Is climate variability over the North Pacific a linear response to ENSO? *J Clim* 9: 1468–1478